Journal of the Australian Ceramic Society (2026) 62:331–355
https://doi.org/10.1007/s41779-025-01258-0

RESEARCH

Investigation of the adhesion properties of duplex coating on AZ91 alloy surface by MAO/HiPIMS-PVD methods

Emine Boynueğri Kaplan[1,2] · **Süleyman Şüküroğlu**[3] · **Ebru Emine Şüküroğlu**[1]

Received: 12 December 2024 / Revised: 24 May 2025 / Accepted: 13 August 2025 / Published online: 21 August 2025

Abstract

This study focuses on enhancing the surface properties and minimizing the mechanical incompatibility between the AZ91 magnesium alloy and the coating by applying CrAlYN/CrYN gradient coatings through the HiPIMS-PVD method, combined with the enlargement of a MgO intermediate layer via the Micro Arc Oxidation (MAO) method. The duplex coating approach was designed to strengthen adhesion and structural integrity between the substrate and the coating. Coating parameters for both MAO and HiPIMS-PVD processes were optimized using a Taguchi L4 orthogonal array, and the coatings were analyzed using SEM, EDS, XRD and scratch testing. MAO coatings exhibited porous and rough surfaces with volcanic morphologies. The best adhesion performance under MAO conditions was achieved with 650 V, 700 Hz, and a Type B solution, resulting in a critical load value of Lc_2 = 24 N. CrAlYN/CrYN gradient coatings alone showed coating thicknesses from 0.83 µm to 1.66 µm with compact and homogeneous microstructures. Adhesive strength was relatively low (Lc_2 = 5–10 N). In the duplex coating configuration, CrAlYN/CrYN coatings were deposited on the MAO-formed MgO layer, significantly increasing adhesion. Critical load values (Lc_2) ranged from 90 to 110 N, with the highest adhesion achieved under low CrY target voltage and current conditions. The findings demonstrate that the MAO/HiPIMS-PVD duplex coating method substantially improves adhesion and surface characteristics of AZ91 alloy, offering a promising solution for advanced surface engineering applications.

Keywords AZ91 magnesium alloy · Micro Arc Oxidation (MAO) · High Power Impact Magnetron Sputtering (HiPIMS) · Duplex coating · Gradient coating

Introduction

The motto of *reduce*, *reuse and recycle* has become a popular contemporary concept alongside developments in energy efficiency and conservation. This has increased demand for new and/or improved products in many industrial fields, such as machinery, automotive, defence and aerospace. This has led to the use of lightweight metals and alloys, such as magnesium (Mg), aluminium (Al) and titanium (Ti), which are popular engineering materials. Light metals and alloys are generally selected for industrial purposes due to their high specific strength and low density. However, their relatively poor surface properties limit their use in critical machine systems or parts. In this context, surface improvement methods are required to enable machine systems made of light metals and alloys to fulfil their functions effectively and extend their service life [1, 2].

In addition to their excellent physical, chemical and mechanical properties, magnesium and its alloys are widely used in industry to meet the demand for lightweight materials in many sectors [3]. These alloys have a wide range of applications in many industrial fields, including automotive, aerospace, electronics and biomedicine, due to their low density, high specific strength, ease of machining and welding, excellent damping properties, large hydrogen storage capacity, and good biocompatibility [4–10]. These advantages, coupled with the convenient recycling of metallic

✉ Ebru Emine Şüküroğlu
eesukuroglu@gumushane.edu.tr

1 Department of Mechanical Engineering, Gümüşhane University, Gümüşhane, Turkey

2 Kastamonu University, Abana Sabahat Mesut Yilmaz Vocational School, Kastamon, Turkey

3 Faculty of Health Sciences, Department of Occupational Health and Safety, Gümüşhane University, Gümüşhane, Turkey

materials, have attracted global interest in magnesium and its alloys. However, their use is limited by some disadvantages, such as low strength at high temperatures and poor corrosion and tribological properties [8, 11, 12]. Examining the literature reveals that many surface treatment techniques are employed to enhance the surface properties of magnesium alloys [6, 8, 12]. One such technique is physical vapour deposition (PVD), which is widely used in industry for various base materials [13].

PVD methods [14] essentially involve growing a solid or molten target material by vaporising or sputtering it onto the base material in a controlled manner. These methods can be used to form single or multilayer coatings that are either thin or thick, ranging in thickness from a few nanometers to thousands of nanometers [15]. Hard coatings with low surface roughness and a low coefficient of friction can be obtained using single or multilayer coatings formed by PVD. Low surface roughness and a low coefficient of friction are important features for tribological and corrosive applications. When the appropriate coating parameters are selected, this method can be used to grow coatings of the desired thickness on the surface of temperature-sensitive base materials such as magnesium and its alloys. In addition to increasing the wear and corrosion resistance of magnesium and its alloys, the service life and commercial value of these materials are significantly increased by the grown coatings [6, 14, 16–18].

To date, PVD coatings, both single-layer and multilayer, such as TiN, AlTiN, AlCrN, AlN, ZrN, CrN, AlN/TiN, TiN/TiCrN, ZrO_2, TiNbTaZr, have been grown on magnesium alloys [19–23]. Li et al. investigated the microstructure and residual stresses of smooth, compact TiN/TiCN multilayer films grown on AZ31 magnesium alloy using DC magnetron sputtering [18]. They determined that TiN/TiCN coatings are smooth and consecutive with small roughness; that the stress is tensile; and that the residual tensile stress value decreases with an increase in the reaction gas ratio, which is one of the PVD process parameters. Sivapragash et al. [21] grew ZrN nanocoatings on AZ91D magnesium alloy surfaces by optimising PVD process parameters (gas type, chamber pressure and power input) using the Taguchi-GA (Genetic Algorithm) method, then investigated the mechanical and tribological properties of these coatings. They found that ZrN-coated AZ91D magnesium alloy has a higher microhardness than untreated alloys and is more resistant to wear mechanisms such as delamination, oxidation, adhesion, and plastic deformation. Çelik and Bozkurt [7] grew Ag-doped TiN and AlTiN coatings on AZ31 magnesium alloy using the PVD method, investigating the relationship between the wear performance of these coatings in simulated body fluid and their biological effects. They performed liquid media experiments under three different solutions (SBF, DMEM and PBS) and two different wear loads. They determined that the hardness of the Ag-doped TiN coatings (1040 HV) was higher than that of the AlTiN coatings (920 HV), the surface roughness of the AlTiN coatings (1.66 µm) was lower than that of the Ag-doped TiN coatings (6.80 µm) and that the coefficient of friction increased in direct proportion to the surface roughness. They concluded that both coatings enhanced the corrosion resistance of the base material.

The most significant disadvantage of PVD-grown coatings is their mechanical incompatibility and low adhesion and corrosion properties with the base material due to the lower elastic modulus and hardness of light metals such as magnesium and its alloys compared to PVD coatings [6, 17, 24, 25]. Weak chemical bonding between the base material and the coating can lead to delamination under cyclic loads, as well as separation and cracking along the coating/base material interface due to high residual stress [15, 26]. Additionally, the weak chemical bond between the coating and the base material can result in high galvanic corrosion [25].

As a result of technological advances, new and/or improved production and coating methods are emerging and developing rapidly. These methods, such as duplex coating prepared by a hybrid process, are used to form thin film coatings and eliminate mechanical incompatibility [16, 24]. One such method is Micro Arc Oxidation (MAO), which is used to grow hard, wear-resistant and chemically bonded oxide coatings on light metallic materials such as magnesium and its alloys [8, 16, 27, 28]. The MAO process is based on an anodic reaction caused by ionisation resulting from plasma micro-discharges on the surface when the electrolytic voltage applied to the base material exceeds the breakdown voltage [27]. The ceramic coatings that result from this process are a combination of oxides from the base material and oxides of the chemical particles present in the electrolytic solution. Consequently, hard, wear-resistant and corrosion-resistant coatings with excellent chemical bond strength are obtained at the interface of the coating and base material [27, 29, 30]. The present study aims to grow an MgO layer using the MAO method to minimise the mechanical incompatibility of HiPIMS-PVD coatings with magnesium alloy.

In this study, CrAlYN/CrYN gradient coating was grown as an interlayer on AZ91 magnesium alloy by MAO method and then the surface properties of magnesium alloy were improved by HiPIMS-PVD coating method. First, an MgO interlayer was grown on the base material using the MAO method according to the L4 experimental plan proposed by the Taguchi test design method. The adhesion strength of the oxide layer grown to the AZ91 base material was then optimised according to the levels of the coating parameters. The new MgO coating, grown using the optimized values, forms the interlayer beneath the CrAlYN/CrYN gradient coating. The CrAlYN/CrYN gradient coating was then obtained on

Table 1 The chemical composition of AZ91 magnesium alloy (% weight)

Alloy	%Mg	%Al	%Zn	%Fe	%Ni	%Cu
AZ91	Bal.	8.7–8.9	0.8–0.9	< 0.005	< 0.001	< 0.001

Table 2 Coatings parameters and levels for MAO

Parameters		Levels	
		1	2
K	Frequency, (Hz)	700	1000
L	Voltage, (V)	500	650
M	Type of electrolyte solution	A	B

Table 3 Taguchi L_4 experimental plan

Experiment No	Levels of Parameters		
	K	L	M
1	700	500	A
2	700	650	B
3	1000	500	B
4	1000	650	A

Table 4 Process parameters and their levels for HiPIMS-PVD coatings

Parameters		Levels	
		1	2
K	CrY Voltage (V)	400	600
L	Al-Target Current	0.5	1.5
M	N_2 Amount (g)	2.5	4.5

the MgO layer using the HiPIMS-PVD coating method. The structural properties of the resulting duplex coating were evaluated using SEM, XRD and EDS analyses, while the adhesion properties were evaluated using a scratch tester. It was observed that the MgO + CrAlYN/CrYN gradient duplex coating, which was optimized for adhesion, eliminated the mechanical incompatibility of the coatings on the AZ91 magnesium alloy with the base material.

Materials and methods

Preparation of the substrates

A 20 × 20 mm² magnesium AZ91 alloy with a thickness of 2 mm was used as the base material. The chemical composition of the AZ91 magnesium alloy is shown in Table 1. The selected samples were polished using SiC sandpaper with grain sizes of 800 and 1200, respectively, until the surface roughness value reached Ra ≈ 0.1 µm. The polished samples were cleaned and dried with ethanol in preparation for coating.

MgO coating using MAO method

The process was performed using an MgO intermediate layer on AZ91 alloys according to the L4 experimental plan from Taguchi test design methods. The frequency, voltage and electrolyte solution, which affect the properties of the coating, were selected as process parameters. Two different electrolyte solutions were prepared to deposit MgO using the MAO method on AZ91 base materials. Electrolyte A contained 8 g of $Na_2SiO_3.5H_2O$ (Sigma-Aldrich, in bead form, molecular weight: 212.14 g/mol and purity: ≥ %95.0), 12 g of Na_2HPO_4 (Sigma-Aldrich, in white crystalline powder form, molecular weight: 141.96 g/mol and purity: ≥ %99.0) and 6 g of KOH (Sigma-Aldrich, in pelet form and purity: %99.99), and Electrolyte B contained 12 g of KOH and the same amounts of $Na_2SiO_3.5H_2O$ and Na_2HPO_4. The coating processes were performed in bipolar mode using an AC power supply for a fixed coating time of 10 min in the specified aqueous solutions produced by Faraday Electronic Corporation. In all experiments, the AZ91 samples were used as the anodes and the stainless steel bathroom wall was used as the cathode. The temperature of the electrolytic solution was cooled by passing water through the stainless steel tank. After the MAO process, the samples were washed and dried in ethanol. According to the Taguchi L4 test plan, four different experiments were carried out at various levels of the selected process parameters in order to optimise the levels of parameters that affect the MAO method. The selected process parameters and their levels are shown in Table 2. The Taguchi L4 experimental plan is shown in Table 3.

CrAlYN/CrYN coating by the HiPIMS-PVD method

The CrAlYN/CrYN gradient was produced using the High Power Impact Magnetron Sputtering (HiPIMS-PVD) method in a physical vapour deposition (PVD) system manufactured by Teer Coating Ltd on AZ91 base materials. These materials were coated using one aluminium (Al) target, one chromium (Cr) target, one chromium-yttrium (CrY) target and two chromium-yttrium (CrY) targets. During the coating process, the base materials were rotated between the aluminium, chromium and yttrium targets at a speed of 2 rev./min. The surfaces were cleaned with 30 min of ionized cleaning just before the coating process. Four different experiments (R1, R2, R3 and R4) were performed at various levels of the selected process parameters according to the Taguchi L4 experimental plan, in order to optimise the levels of parameters affecting the HiPIMS-PVD process. The selected process parameters and their levels are shown in Table 4. The Taguchi L4 experimental plan is shown in Table 4. The Taguchi L4 experimental plan is shown in Table 5.

Table 5 Taguchi L_4 experimental plan

Experiment No	Levels of Parameters		
	K	L	M
R1	400	0.5	2.5
R2	400	1.5	4.5
R3	600	0.5	4.5
R4	600	1.5	2.5

While coating AZ91 base materials with the HiPIMS-PVD method, the experiments were performed in pulsed direct current mode. Following ionised cleaning during the coating process at a Cr operating pressure of 2.5×10^{-3} Torr for 10 min, the following fixed parameters were selected: CrN for 15 min, CrAlYN for 20 min and CrYN for 30 min at an operating pressure of 3×10^{-3} Torr.

Duplex coatings

MgO coatings, created using the Taguchi test design method in a series of experiments and enlarged on AZ91 base materials, were systematically evaluated, with the results of each condition optimised in terms of adhesive properties. The optimum conditions were verified according to the levels of the determined parameters, with the highest adhesion value being reached in the output. New coatings were made under the conditions determined by this experiment using the MAO method. Each sample was made according to the coating conditions shown in Tables 4 and 5, based on four different experimental plans shown in Table 4. Duplex coatings were obtained by creating a CrAlYN/CrYN gradient coating according to the conditions in Table 4.

Characterisation of the coatings

An X-ray diffractometer (XRD) was used to detect the phases in the structure of the materials after the AZ91 base material and MAO processes. XRD measurements of MgO coatings generated on AZ91 base material were performed using a Panalytical Empyrean model XRD device with Cu-Kα radiation at a wavelength of $\lambda = 1.5404$ Å.

The AZ91 base material was coated with MgO using the MAO method. A scanning electron microscope (SEM) was used to determine the surface morphology and coating thickness of CrAlYN/CrYN samples coated by the HiPIMS-PVD method. The chemical composition of the CrAlYN/CrYN gradient coats coated using the HiPIMS-PVD method was analysed using an energy-dispersive X-ray spectrometer (EDS), which was integrated into the same device.

The adhesion of the coating to the base material of the MAO intermediate layer and the CrAlYN/CrYN gradient coatings was measured using a ReveTester test device produced by CSM Instruments. Adhesion tests were performed at shift rates of 10 mm/min and 100 N/min under increasing load using a Rockwell C cone diamond indenter with a radius of 200 µm.

Optimisation of the experimental parameters

The optimisation process focused on adhesion of the enlarged coatings, using the Taguchi test design method. Within the scope of this thesis, the data collected from scratch tests performed on the enlarged MgO coatings were analysed using the ANOVA-TM package program. 'Performance statistics' were selected as the optimisation criterion. To observe the effects of the parameters on the optimisation criterion, a review of the literature was conducted. According to the results of the scratch tests, the Lc2 value was based on the critical load of the coatings in the adhesion tests. For the Lc2 critical load value, 'larger is better' performance statistics were used. The study determined the experimental requirements with the optimum Lc2 value. The effect of each parameter on the optimisation criterion was calculated, and the results were presented in graphics and charts. The optimisation process has been completed, meaning that the numerical value of the maximum points on the graphs shows the optimum value of the relevant parameter, while the numerical value of the minimum points shows the worst value according to 'larger is better' performance statistics.

Results and discussion

Optimisation of structural and adhesion properties of MgO coatings

Figure 1 shows the surface morphologies of the coatings produced after the MAO process was applied to the AZ91 alloy in accordance with the Taguchi L4 experimental plan. Figure 2 presents cross-sectional images of the coatings. Images taken from the coating surface using a scanning electron microscope (SEM) show that the oxide structure is distributed evenly across the entire surface. Examination of the SEM images reveals that the coatings on AZ91 in the MAO process, depending on micro-eliminations (discharge), have a rough surface with a large number of micro-cavities (pores) of various diameters, as well as volcanic formations caused by micro-meltings. This result is consistent with related literatüre [31–33].

Zhang et al. [34] stated that a circular pathway of regional melting, followed by solidification, caused the micro gaps formed in the coating to be almost circular in geometry. In the MAO method, the applied voltage causes the formation of discharge ducts, enabling the growth of the coating layer by locally exceeding the dielectric breakdown voltage

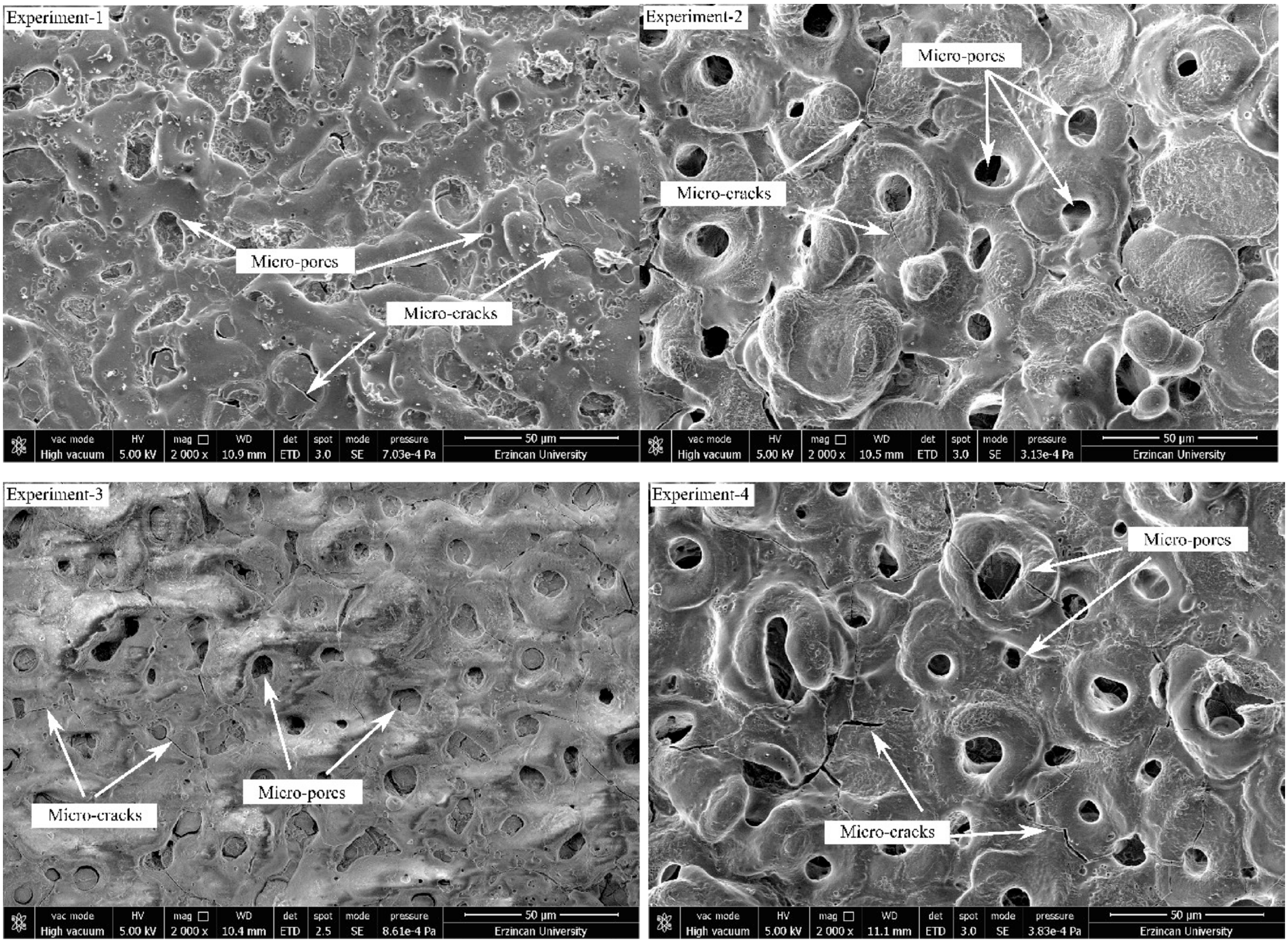

Fig. 1 Surface morphology of the coating grown using the MAO method on AZ91 alloy in all Experiments

on the surface of the enlarged oxide coating (as shown in Fig. 6). The resulting discharge creates high pressure and temperature within the discharge duct, allowing the coating to form. The high pressure and temperature during coating formation cause melting and evaporation in some regions, forming circular or nearly circular gaps on the coating surface near the gaps formed by discharge ducts [32, 35].

Examining the surface morphology of the coatings in Fig. 1 in detail reveals that there are many circular micro-gaps with a fairly uniform distribution across all samples. Examining the sample images of the micro-gaps at the same enlargement rate reveals that the dimensions of the pores and their dispersion on the surface change depending on the experimental parameters. The number of micro gaps is lower and their diameters are smaller in experiment 1 (700 Hz, 500 V, Type A solution). This is thought to arise from the progression of current values that remain at very low levels throughout the coating period compared to other experiments [33]. Hussein et al. [36] stated that the dimensions of the micro-gaps are related to the energy formed on the surface, which can be controlled by various coating parameters. Additionally, studies examining the effect of frequency on surface morphology have shown that the number of micro gaps increases while their diameters decrease as the frequency increases [33, 37, 38]. Martin et al. [39] explained the reason for the differences in the uniform and non-uniform distribution of the micro-gaps, stating that these resulted from local melting within the arc ducts and the distribution of molten material. The relevant literature clearly shows that coating parameters affect the structure of micro-gaps on the coating surface. The effect of frequency, voltage, processing time and solution concentration on coating morphology is quite remarkable in the MAO process [40].

Figure 2 shows cross-sectional images of the coatings enlarged at different parameters on AZ91 alloy. Additionally, the coating thickness was measured at different points using SEM images of the samples, and the average values are shown in Fig. 2. The lowest average coating thickness was obtained in experiment 1 at approximately 26 µm, while the highest was approximately 60 µm in experiment 2. It is thought that the coating parameter levels and the

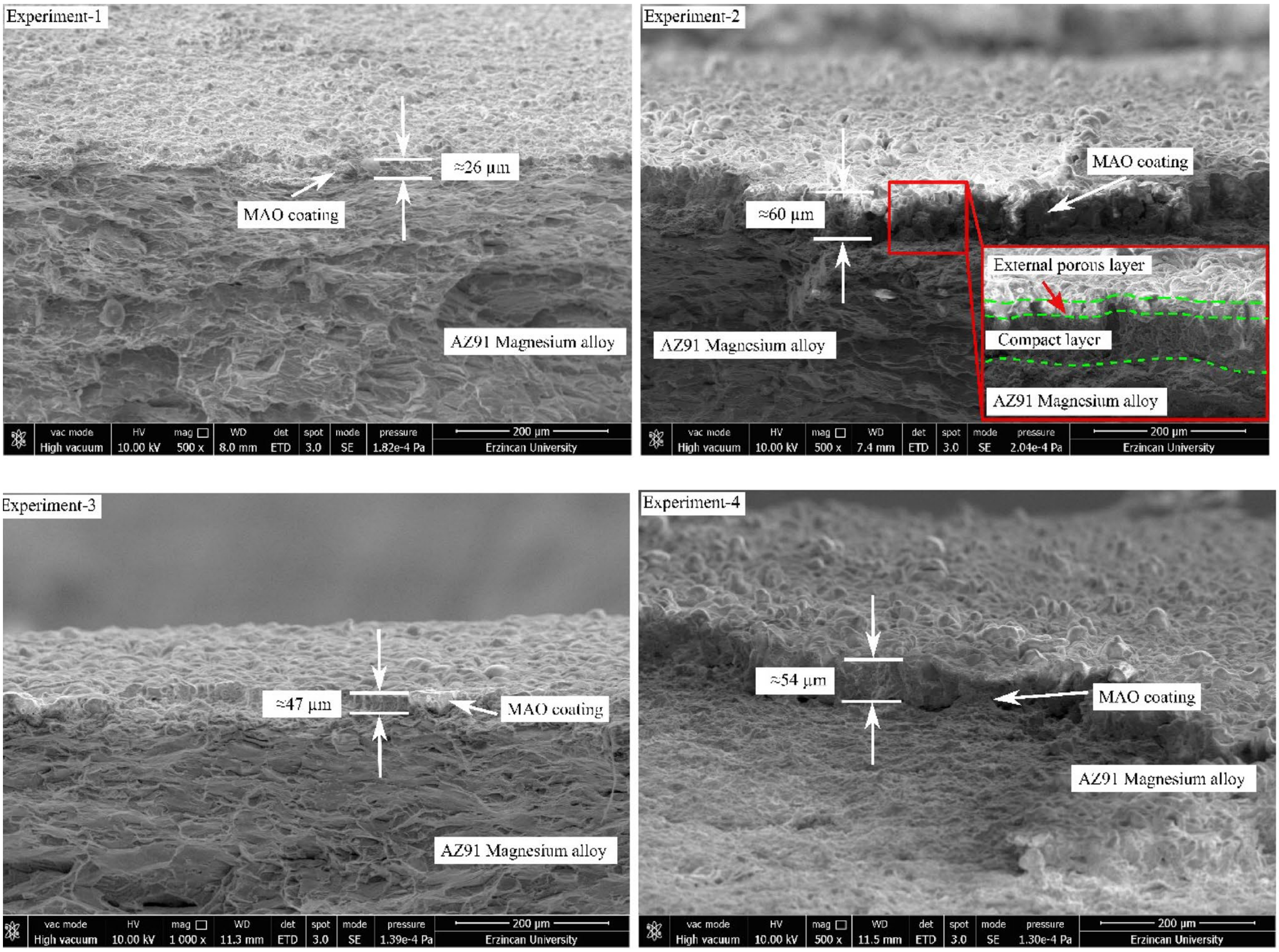

Fig. 2 The cross-sectional view of the coating grown by the MAO method on AZ91 alloy under the conditions of all experiment

phase structures produced by these parameters are effective in determining the coating thickness. Figure 2 shows the three-layered structure of the MAO coating in detail. It is difficult to clearly determine the flimsy barrier layer formed on the base material using SEM images alone. However, the thick main MAO layer located just below the porous surface with a large number of micro-gaps can be clearly seen. The SEM images obtained are consistent with the literature [36].

Figure 3 shows the XRD graphs of the coatings enlarged according to different parameters, substrates (AZ91 alloy), the MAO method and the Taguchi experimental plan. The literature reports in detail that MgO is formed by the MAO method in different crystal structures [32, 41–44]. These studies emphasise that the basic phase formed as a result of MAO coatings on magnesium alloys is MgO. Chen et al. [45] stated that the high temperatures formed during the MAO coating process allow the MgO phase to form. They also revealed that the chemicals in $Na_2SiO_3.5H_2O$, Na_2HPO_4 and KOH aqueous solutions formed Mg_2SiO_4 and Mg(PO_4 phases in the XRD analysis of MAO-coated samples. Liang et al. [46] found that MgO and Mg_2SiO_4 phases occurred in the structure of the coatings in experiments performed in $Na_2SiO_3.5H_2O$ + KOH aqueous solutions. The XRD analyses in this study revealed other small peaks, which are thought to be caused by elements in the alloy. Different phases can also be obtained depending on the chemical composition of the solution used.

However, it is very difficult to obtain these phases by XRD analysis. The XRD results indicate that the MgO phases at $2\theta = 36.39°$, 38.02°, 42.98°, 62.36°, 74.71° and 78.66° were found to be much more abundant in experiments 2 and 4 than in the other experiments. This is reflected in the thickness of the oxide layer when the enlarged coatings are examined together. Similarly, Fig. 3 shows that the Mg_2SiO_4 and Mg(PO_4) phases, which are thought to be caused by the chemicals in the solution, had a higher intensity in experiments 2 and 4. This demonstrates the significant impact of different frequencies, voltages, and solutions on the coating structure. The results obtained by XRD analysis are consistent with those reported in the literature [33, 43].

In terms of the performance of coatings whose substrate is enlarged, the coating and adhesion are of great importance

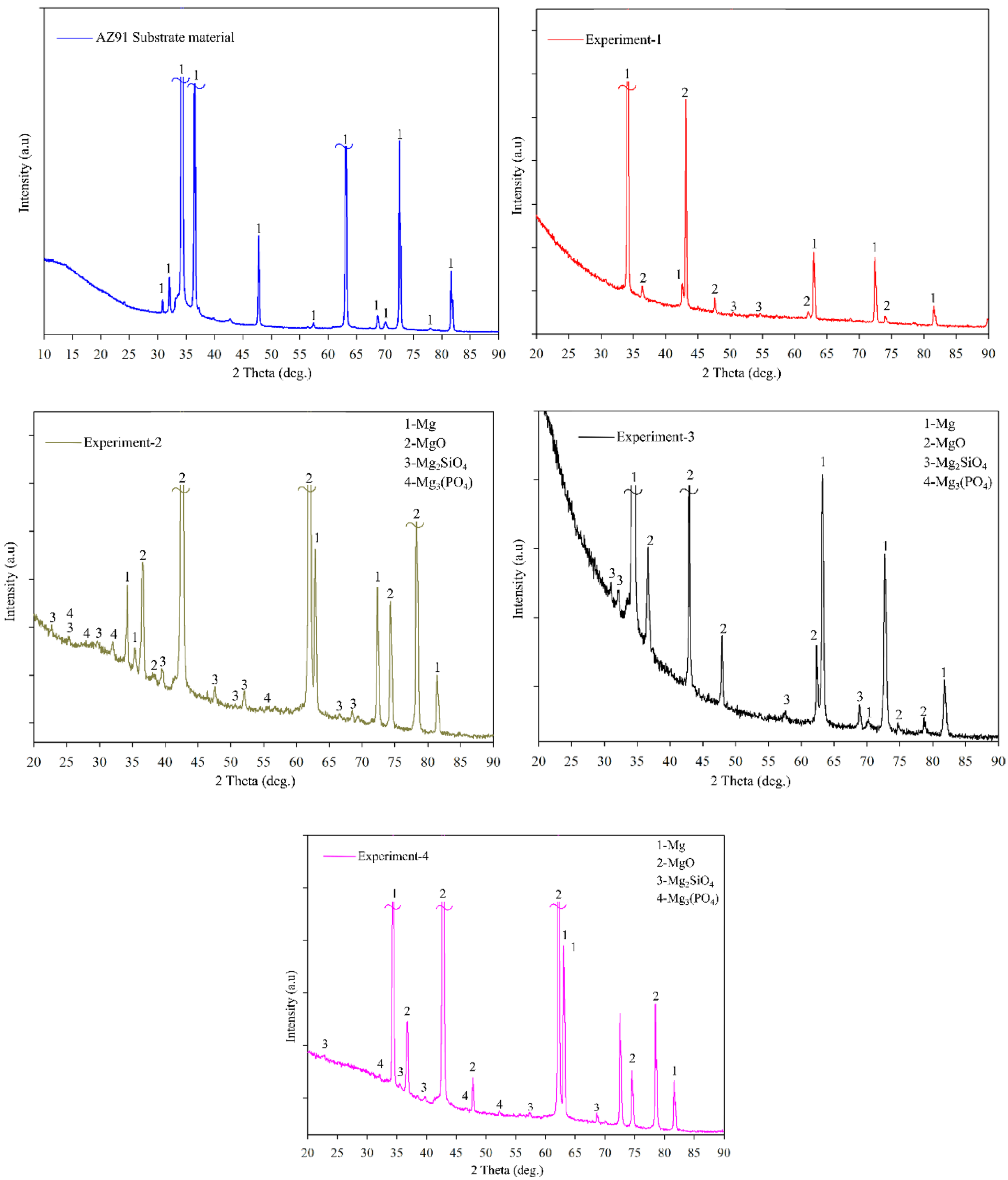

Fig. 3 XRD analysis of the AZ91 magnesium alloy and of the coatings grown by the MAO method on the AZ91 alloy in all experiments

in surface engineering and design. One of the most commonly used methods to measure adhesion between the base material and the coating is the scratch test [47]. In this study, the increased load scratch test (progressive load scratch) was used to measure the adhesion between the AZ91 alloy and the coating after the MAO process. During the scratch test, the coating surface is scratched with a diamond tip under a linear force, and the force caused by the resulting damage is

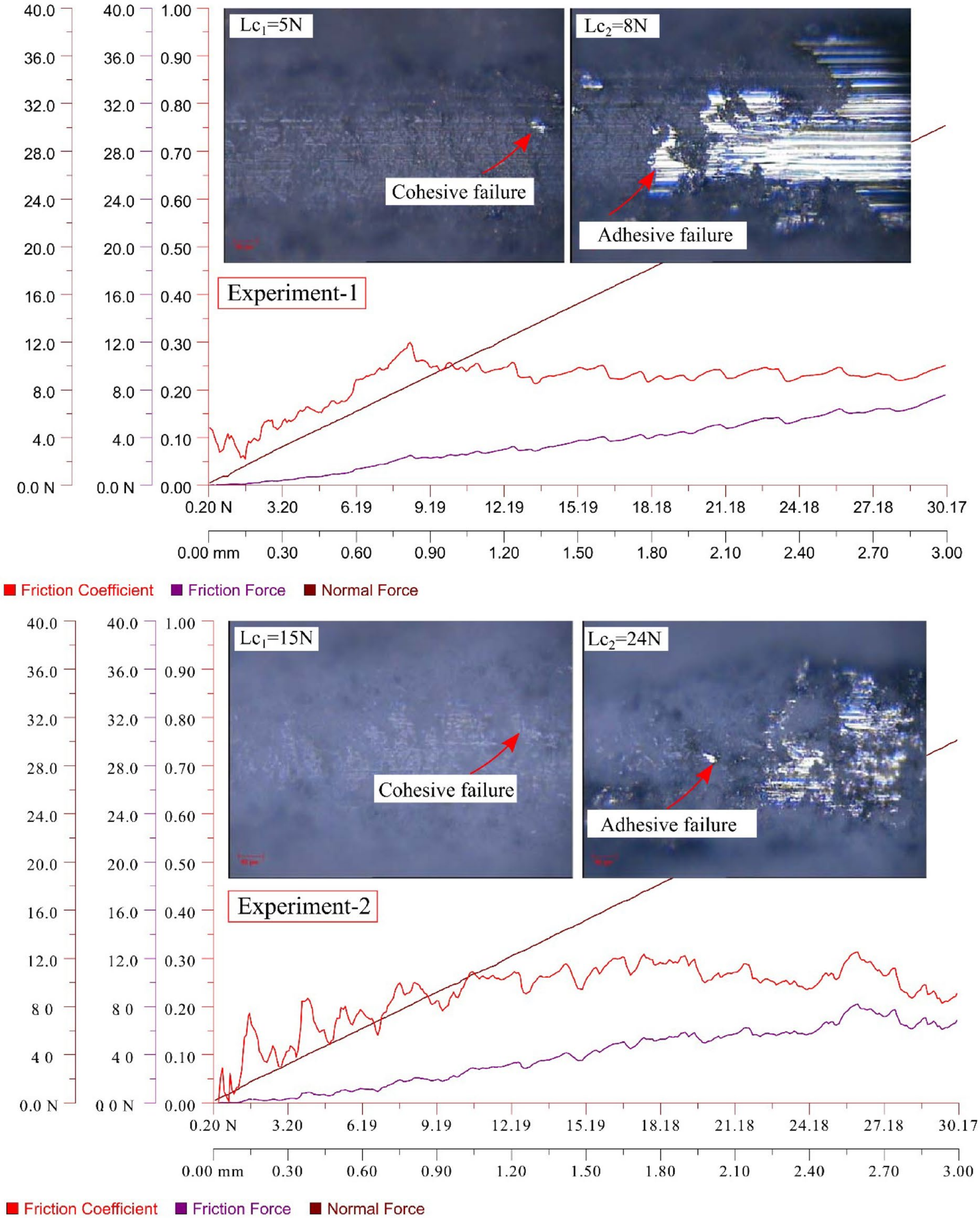

Fig. 4 Scratch test of coatings grown using the MAO method on the AZ91 alloy for all experiments

determined. This force is defined as Lc(Critical Load) and is considered to be the adhesion force between the coating and the base material. Four different critical loads (Lc_1, Lc_2, Lc_3 and Lc_4) are defined as the coating is damaged. In the literature, the Lc_2 value is based on the critical load of oxide coatings in adhesion tests [47].

According to the Taguchi experimental plan, Fig. 4 shows the curves depicting the change in normal load in relation to friction force, as obtained from the scratch test of MgO

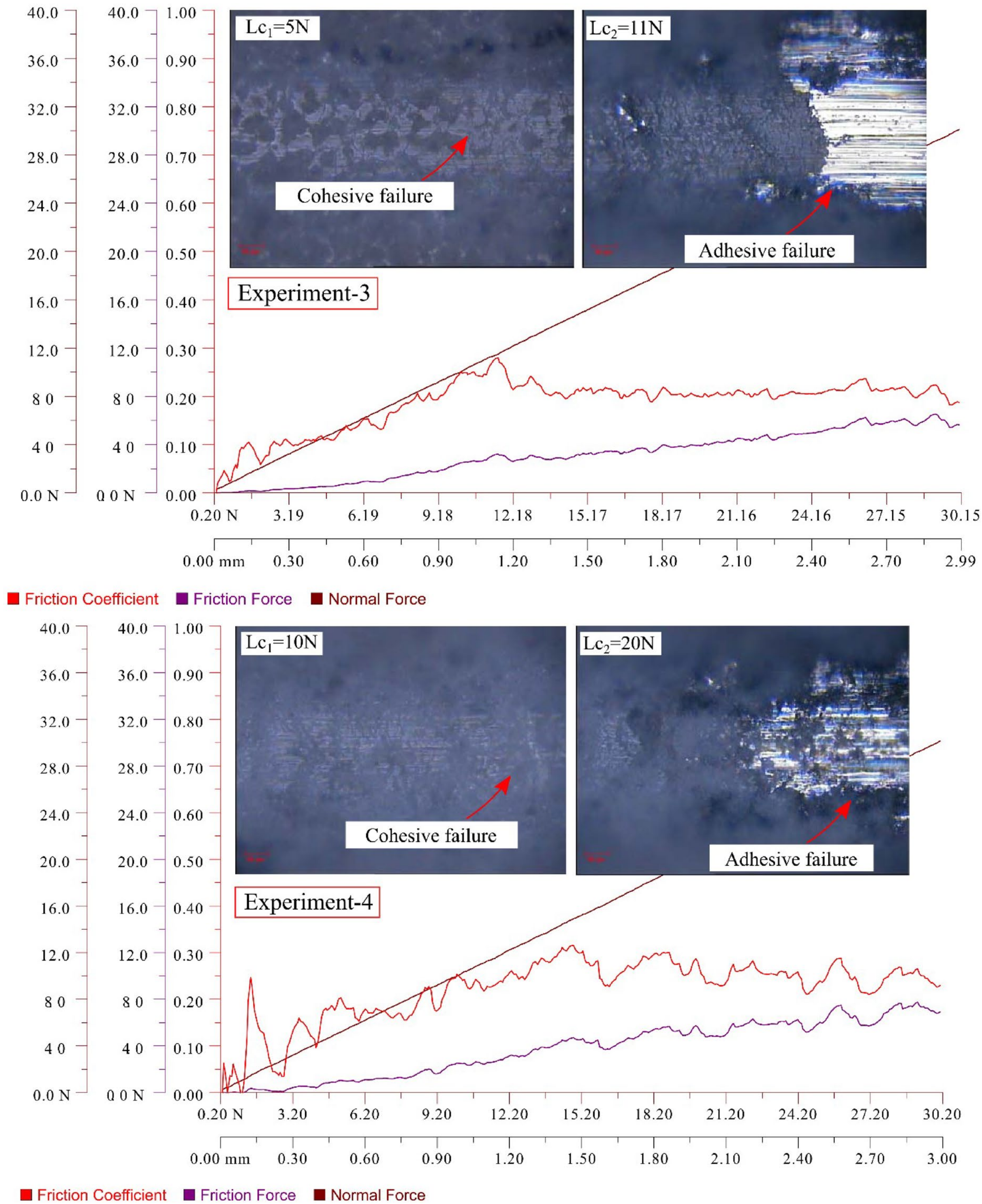

Fig. 4 (continued)

coatings on AZ91 alloy at various parameters and levels. In this study, the Lc2 value was considered to represent the adhesion force that damages the coatings. The scratch test involved applying increased loads to each sample, starting from 0.2 N and increasing to a maximum of 30.2 N. It was found that the Lc1 values, which indicate cohesive strength, ranged from 0 to 5 N in experiments 1 and 3, and increased to between 10 and 15 N in experiments 2 and 4. The highest critical load frequency was 700 Hz for Type B (3 g/L) solution and 650/–150 V for experiment 2, with $Lc_2 \simeq 24$ N.

The MAO coatings with the highest Lc_2 value in experiment 2 can be explained by coating density and phase

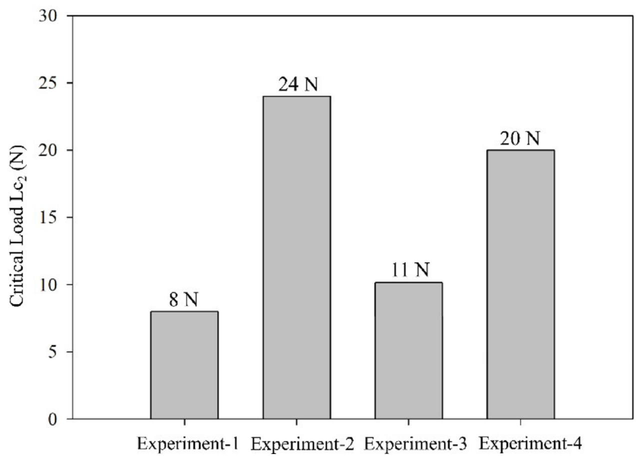

Fig. 5 Critical load values (Lc_2) of coatings grown by the MAO method on AZ91 alloy at different parameters and levels

structure (Mg_2SiO_4 and $Mg(PO_4)$ as shown in Fig. 3). The Mg_2SiO_4 and $Mg(PO_4)$ phases, which are denser than in the other experimental conditions, are thought to increase adhesion between the base material and the coating. Examining the enlarged coatings under the conditions of experiment 2 reveals that their microstructure is denser than that of other coatings (see Fig. 1). In the study by Demirci et al. [32], it was found that the thickness of the oxide coating increased with the load-carrying capacity of the coatings, thus increasing adhesion resistance. Figure 5 shows Lc_2 values.

The results obtained from the scratch test on the AZ91 alloy after the MAO process were optimised using the Taguchi experimental design method. When evaluating the adhesion of the enlarged MAO layers to the base materials, the parameters that were most effective in achieving the highest critical load value (Lc2) were voltage, solution type and frequency, respectively. According to these performance statistics, the Taguchi test design method proposed the following values: frequency (700 Hz), Type B solution (3 g/L) and voltage (650/-150 V), as determined in Experiment 2.

The test results obtained from the scratch test after the MAO process on the AZ91 alloy were optimised using the Taguchi test design method. It is known that two basic parameters affect the performance of the MAO process. These parameters are categorised as electrical or electrolytic variables [33]. The electrical variables include the type of power supply, current density, discharge current type, duty cycle, duty time, frequency and applied voltage. Electrolytic variables include the type, temperature and pH of the electrolyte [32]. Following preliminary attempts and a review of the literature, the most effective parameters and their levels were selected for the MAO process, and MAO coatings were applied to the AZ91 alloy according to the Taguchi L4 experimental plan given in Table 5.

Data obtained from scratch tests performed on MgO coatings enlarged on the AZ91 base material were analysed using the ANOVA-TM package program. 'Performance statistics' were selected as the optimisation criterion. To determine the effects of the parameters on the optimisation criterion, the Lc_2 value was considered the critical load in adhesion tests of the coatings, according to the results of the scratch tests. For the Lc_2 critical load value, 'larger is better' performance statistics were used [32]. The aim of the process was to determine the optimum Lc2 value for the experimental conditions. The effect of each parameter on the optimisation criterion was calculated, and the performance statistics were displayed in graphics and tables. The optimisation process has been completed, with the numerical value of the maximum points in the graphics showing the optimum value of the relevant parameter, and the numerical value of the minimum points showing the worst value according to 'larger is better' performance statistics.

Examination of the values shown in Table 7, one of the outputs of the ANOVA-TM program, revealed that the most effective parameter for the MAO process was the 'voltage value', symbolised by L. The electrolytic solution type, symbolised by M, was found to be the second active parameter.

Table 6 shows the statistical values of the data obtained under all the experimental conditions of the ANOVA-TM programme. When the adhesion of the MAO coatings on the AZ91 base material was evaluated, the parameters with the greatest impact on the critical load value (Lc2) were identified as voltage, electrolytic solution type and frequency, respectively (Fig. 6).

According to these performance statistics, the Taguchi test design method proposed for the largest Lc_2 value includes B-type electrolytic solution, a voltage of 650 V, and a frequency of 700 Hz. These results were found to

Table 6 Statistical data of the ANOVA-TM package program

Experiment No	Data	Total	Mean	S(squares)	S(squares)	Variation	S(squares)	Variance
	n	t	m	Ss	Sr	St	Sm	Ve
1	1	8.0000	8.0000	64.0000	0.0156	0.0000	64.0000	0.0000
2	1	24.0000	24.0000	576.0000	0.0017	0.0000	576.0000	0.0000
3	1	11.0000	11.0000	121.0000	0.0083	0.0000	121.0000	0.0000
4	1	20.0000	20.0000	400.0000	0.0025	0.0000	400.0000	0.0000
All data	**N**	**T**	**M**	**SS**	**SR**	**ST**	**SM**	**VE**
	4	63.0000	15.7500	1,161.0000	0.0281	168.7500	992.2500	56.2500

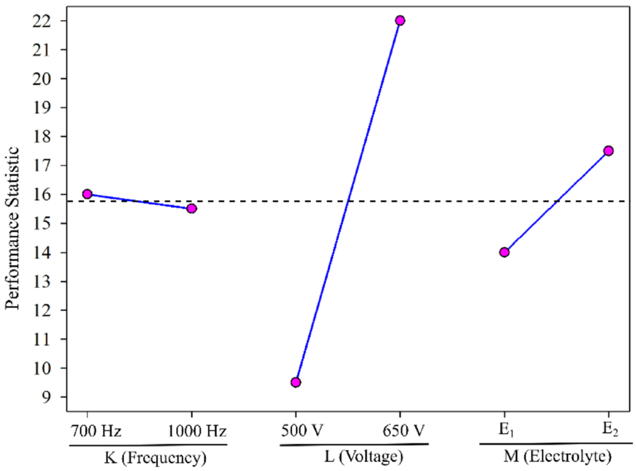

Fig. 6 Performance statistics plot affecting the adhesion of MgO coatings grown on AZ91 alloy

align well with the experimental plan made in accordance with the L4 orthogonal series.

The confidence interval was evaluated for the difference between the estimated and found values. Here, the estimated error is the relationship between the theoretical experimental conditions, the application of the verification experiment, and the values found. The confidence interval for the estimated error was calculated using the ANOVA-TM package program. The adhesion properties optimised using the Taguchi experimental design method were found to lie within the 95% confidence interval. As the performance values obtained in the verification experiments fall within the calculated confidence interval, the experimental results can be considered acceptable at a 5% error level. This process is consistent with the literature [32].

Structural and adhesion properties of CrALYN/CrYN gradient coatings grown on AZ91 alloy by the HiPIMS-PVD method

Figure 7 shows SEM images of the coatings enlarged at different parameters and levels. Examination of the SEM images reveals that the lowest coating thickness was obtained in R1 test conditions at t ≃ 0.83 µm, as shown in Fig. 7, while the highest coating thickness was obtained in

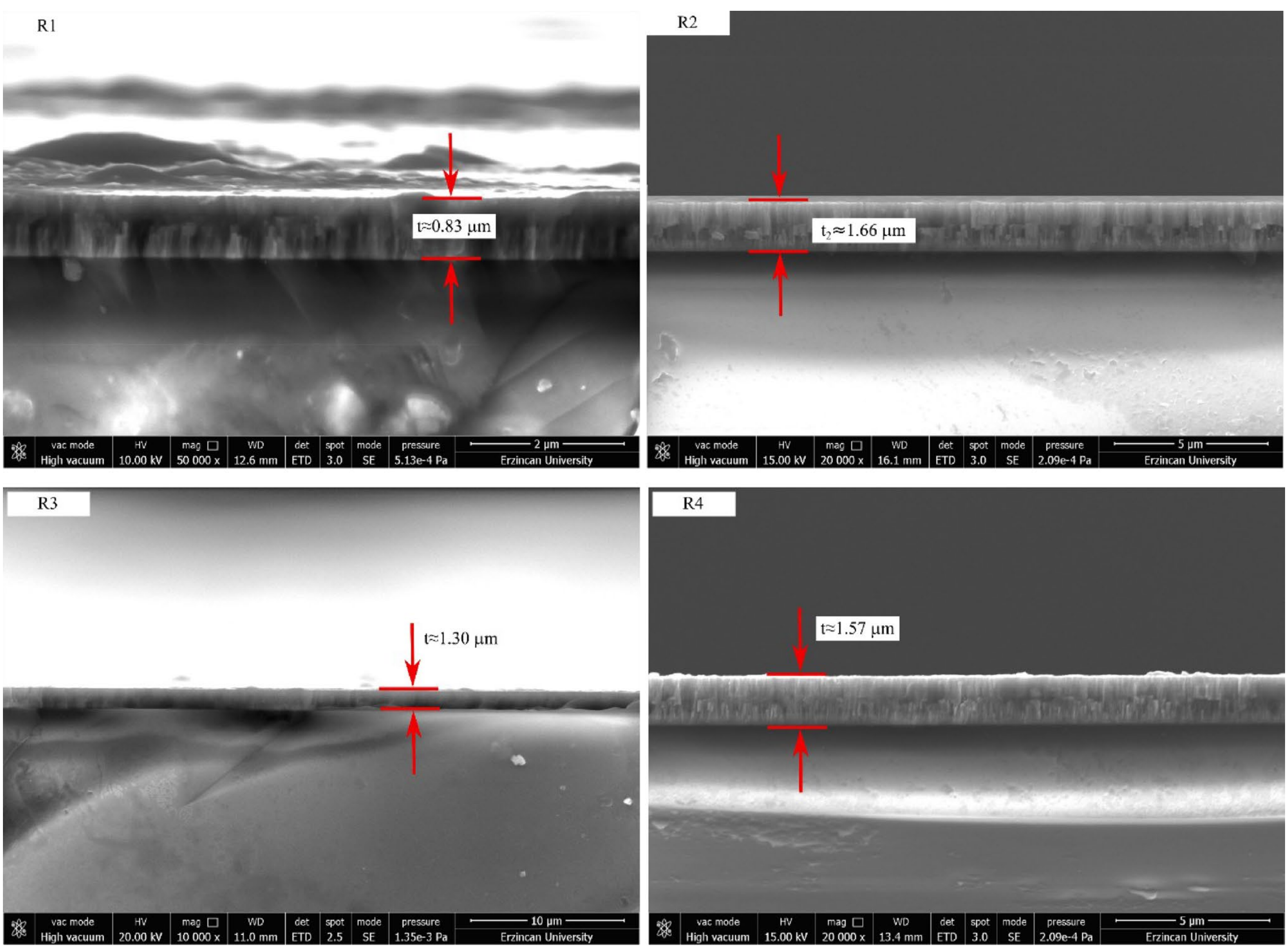

Fig. 7 Cross-section SEM image of a CrAlYN/CrYN gradient coating grown by HiPIMS-PVD method on a glass substrate under R1-4 conditions

Table 7 Order of influence of parameters on adhesion properties

	K	L	M
Level 1	16.0000	9.5000	14.000
Level 2	15.5000	22.0000	17.5000
Delta	0.5000	12.5000	3.5000
Rank	3	1	2

R2 test conditions at t ≃ 1.66 µm. The coating thickness values for all tests are shown in Fig. 7. Under R2 test conditions, the highest thickness value was detected at levels where the voltage applied to the CrY target was 400 V, the target current applied to the Al target was 1.5 A and the amount of N_2 was 4.5 g, according to the parameters affecting CrAlYN/CrYN coatings. Examining the four different experimental conditions (R1, R2, R3 and R4), it was found that the target current applied to the Al target and the amount of N_2 (g) given to the system in the R2 conditions resulted in the highest coating thickness (as shown in Table 4 and 5).

Examining the existing literature, it is evident that there is a decrease in the thickness of fine films as the amount increases. Aihua et al. [48] explained that this decrease is due to the reactive gas forming a nitride phase on the target surface as the amount of N_2 increases. This nitride layer reduces the splashing rate of the target material. However, although the amount of N_2 given to the system in experiment 2 is higher than in the other conditions (R1 and R4), the higher coating thickness (t ≃ 1.66 µm) clearly plays a more active role in determining the thickness of the coating produced by the target current. He et al. [49] stated that, with an increase in the current value applied to the target materials, an intensive columnar structure was obtained in the coating layer, resulting in an increase in the coating thickness.

When the coatings obtained under the R1, R2, R3 and R4 experimental conditions were examined, they were found to have a very dense, homogeneous, smooth and compact microstructure. In addition to achieving the ideal coating thickness, an intensive microstructure is an important parameter for hardness. Liu et al. [35] stated that itrium (Y) atoms replaced chromium (Cr) and aluminium (Al) atoms in the CrAlN cage structure, forming a solid solution coating. They also suggested that CrAlYN coatings possess conical particles and columnar structures in their surface and cross-sectional morphology. Qi et al. [50] stated that, in CrAlYN coatings, the size of the conical particles and the width of the columnar structures in the cross-sectional structure decreased with an increasing Y ratio (see Fig. 7 for SEM images).

The EDS analysis results for CrAlYN/CrYN gradient coatings enlarged using the HiPIMS-PVD method on an AZ91 alloy are shown in Fig. 8. EDS analysis of CrAlYN/CrYN gradient coatings, produced under the same conditions, was performed on glass substrates. According to EDS analyses taken from the surface of the coatings, the atomic quantities of Cr, Al, Mg, Y and N are given in Fig. 8. Under R2 experimental conditions, the aluminium content in the CrAlYN/CrYN coatings is higher than in the other tests (see Table 4). This can be considered an indicator of increased coating thickness. The literature shows that increasing the current value applied to target materials can increase coating thickness to a certain extent [49–51].

Figure 9 shows the XRD analysis results for CrAlYN/CrYN gradient coatings. The phase structure of CrAlYN/CrYN gradient coatings shows the formation of CrN, AlN and Cr_2N phases. XRD analysis revealed that the presence of CrN and AlN phases at 2θ ≃ 37° and 2θ ≃ 44°, respectively, was significantly higher in intensity in R1, R2 and R4 experimental conditions than in R3 when CrAlYN/CrYN coatings enlarged on glass materials were examined together. The presence of the Cr_2N phase was also observed in R3. Ma et al. [52] enlarged CrAlYN/CrYN gradient coatings on Ti6Al4V base materials using the HiPIMS-PVD method, determining that high-intensity CrN and AlN phases occur in the coatings' structure. This finding is consistent with results from similar studies [35, 51–54].

According to the Taguchi test plan, Fig. 10 presents the results of the scratch test of CrAlYN/CrYN gradient coatings on AZ91 base materials at different levels and parameters. The Lc2 value is considered as the adhesion force that damages the CrAlYN/CrYN gradient coatings. Figure 10 shows a graph of the Lc2 force values for all the enlarged CrAlYN/CrYN gradient coatings on the AZ91 base material. The scratch test involved applying increased loads to each sample, starting from 0.2 N and increasing to a maximum of 50.2 N. The Lc1 values, which indicate cohesive strength, ranged from 0 to 5 N across all experimental conditions, while the Lc2 values, which indicate adhesive strength, ranged from 5 to 10 N. Examination of the scratch test results revealed that the critical load value was approximately 8 N in the experimental condition where the highest Lc2 value, which defines adhesive damage to the CrAlYN/CrYN gradient coatings enlarged on the AZ91 alloy, was obtained. The critical load values were similar in the R1 and R4 conditions (Lc2 ≃ 8 N), while they were lower in the R2 and R3 conditions (Lc2 ≃ 7 N). The results revealed that the adhesion strength between the CrAlYN/CrYN gradient coatings and the AZ91 alloy base materials was very low. This thesis study therefore focused on enlarging CrAlYN/CrYN gradient coatings and MgO intermediate layers using HiPIMS-PVD and MAO methods, with the aim of minimising mechanical incompatibility between the base material and the coatings.

Fig. 8 EDS analysis of CrAlYN/CrYN gradient coating grown by HiPIMS-PVD method on glass substrates under R1-R4 experimental conditions

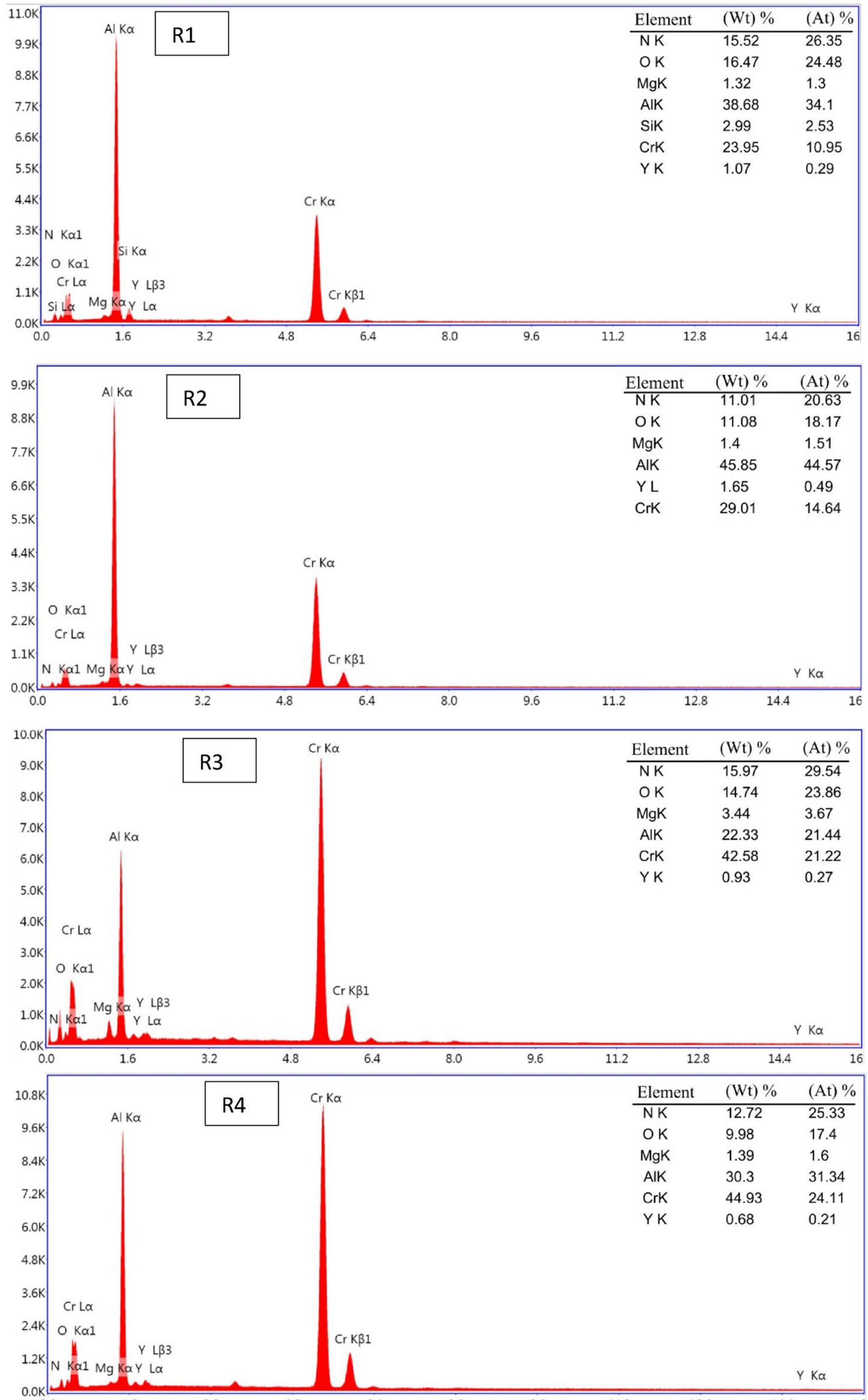

Optimisation of adhesion and structural properties of duplex coatings enlarged on AZ91 by HiPIMS-PVD method

According to the Taguchi L4 experimental plan, the optimum conditions were determined by analysing the results of the scratch test of the MgO coatings enlarged on the AZ91 alloy using the MAO method. The MgO layers were enlarged on AZ91 base materials using the MAO method according to the levels of the specified parameters. Following this, the CrAlYN/CrYN gradient coatings were enlarged using the HiPIMS-PVD method, after which duplex surface

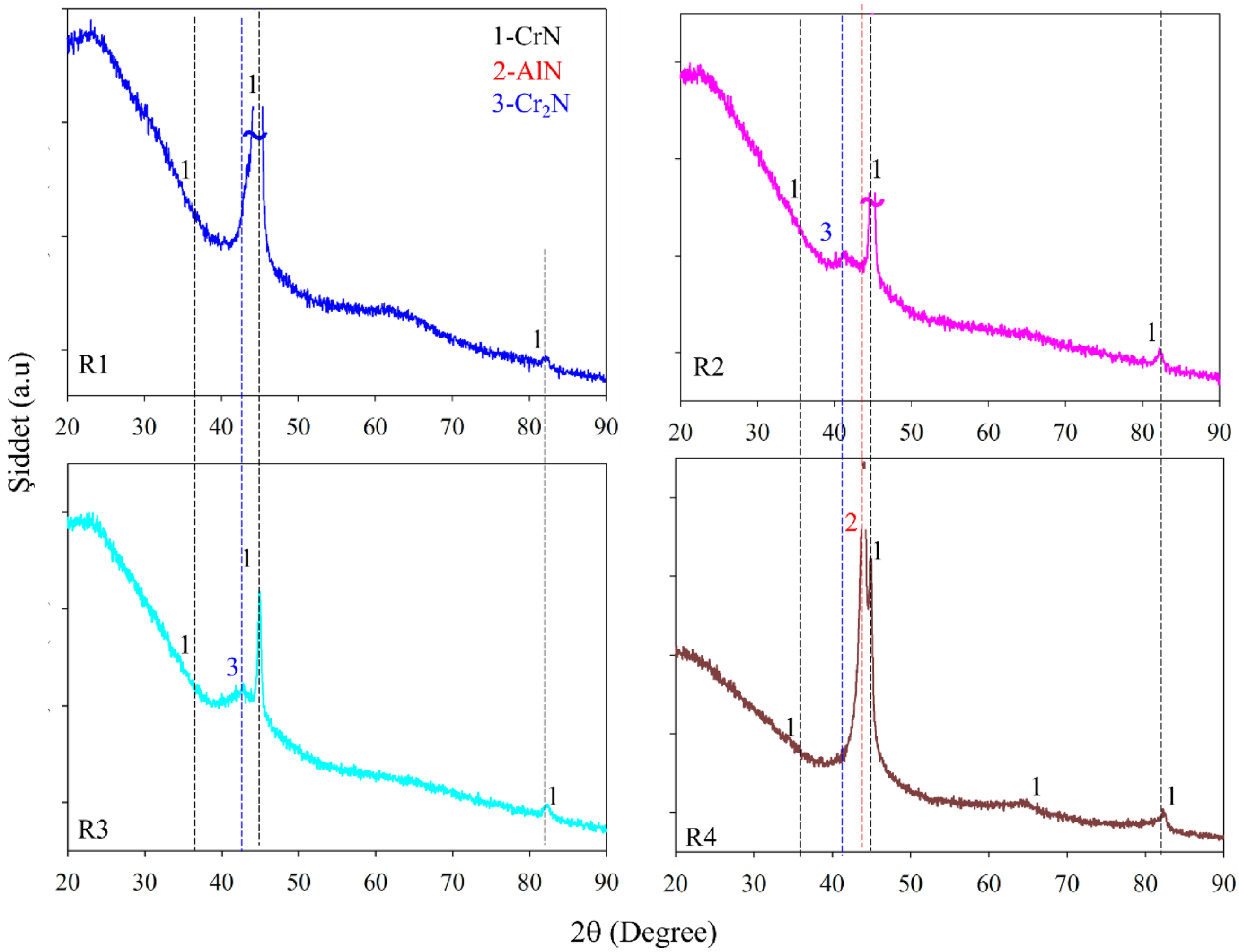

Fig. 9 XRD analysis of CrAlYN/CrYN gradient coatings grown on glass substrate by HiPIMS-PVD method under R1-R4 experimental conditions

processing was performed. The thickness of the coatings was determined using SEM images taken from the cross-sectional surface of the duplex coatings. SEM images of the duplex coatings enlarged on the AZ91 alloy are presented in Fig. 11. As can be seen in Fig. 11, a prominent line formed where the MAO layer separated from the base materials, and the CrAlYN/CrYN gradient coatings that were enlarged under four different experimental conditions on this layer were found to grow in a columnar structure with a very dense, homogeneous, smooth and compact microstructure.

According to the Taguchi L4 test plan, the EDS analysis results for the duplex coatings on the AZ91 alloy are presented in Fig. 12. In the R1, R2, R3 and R4 experimental conditions, the presence of Al and Cr, which are believed to originate from the Al, Cr and CrY target materials, was determined. In the R2 experimental conditions, the aluminium content was higher than in the other conditions. As shown in Fig. 11, the highest coating thickness was obtained in the R2 conditions. However, carbon was present in the R2 and R4 conditions. In both of these conditions, the current value applied to the target was 1.5 A, which, in addition to being higher than in the other conditions, increased the amount of aluminium by percentage, allowing the formation of carbon. It is thought that phosphorus (P) formed in the R3 conditions and silicon (Si) formed in the R1 and R3 conditions derived from the electrolytic solutions used to create the MAO oxide layer.

XRD analysis of the duplex coatings on the AZ91 alloy was performed within a screening range of 20–90°, with a screening step of 0.1° and a screening rate of 2.5°/min. The results of the XRD analysis of the duplex coatings produced using the MAO/HiPIMS-PVD method under the R1, R2, R3 and R4 experimental conditions are presented in Fig. 13. The XRD analysis showed that these coatings contained CrN, AlN, Cr_2N, CrAlYN and CrY. The intensity of CrN was particularly high in the R1, R2, R3 and R4 experimental conditions. However, the SHP-AlN phase was also found to be present in the coating structure. Myandoab [55] stated that the formation of the AlN phase was caused by excessive nitrogen in the coating environment. He also explained that

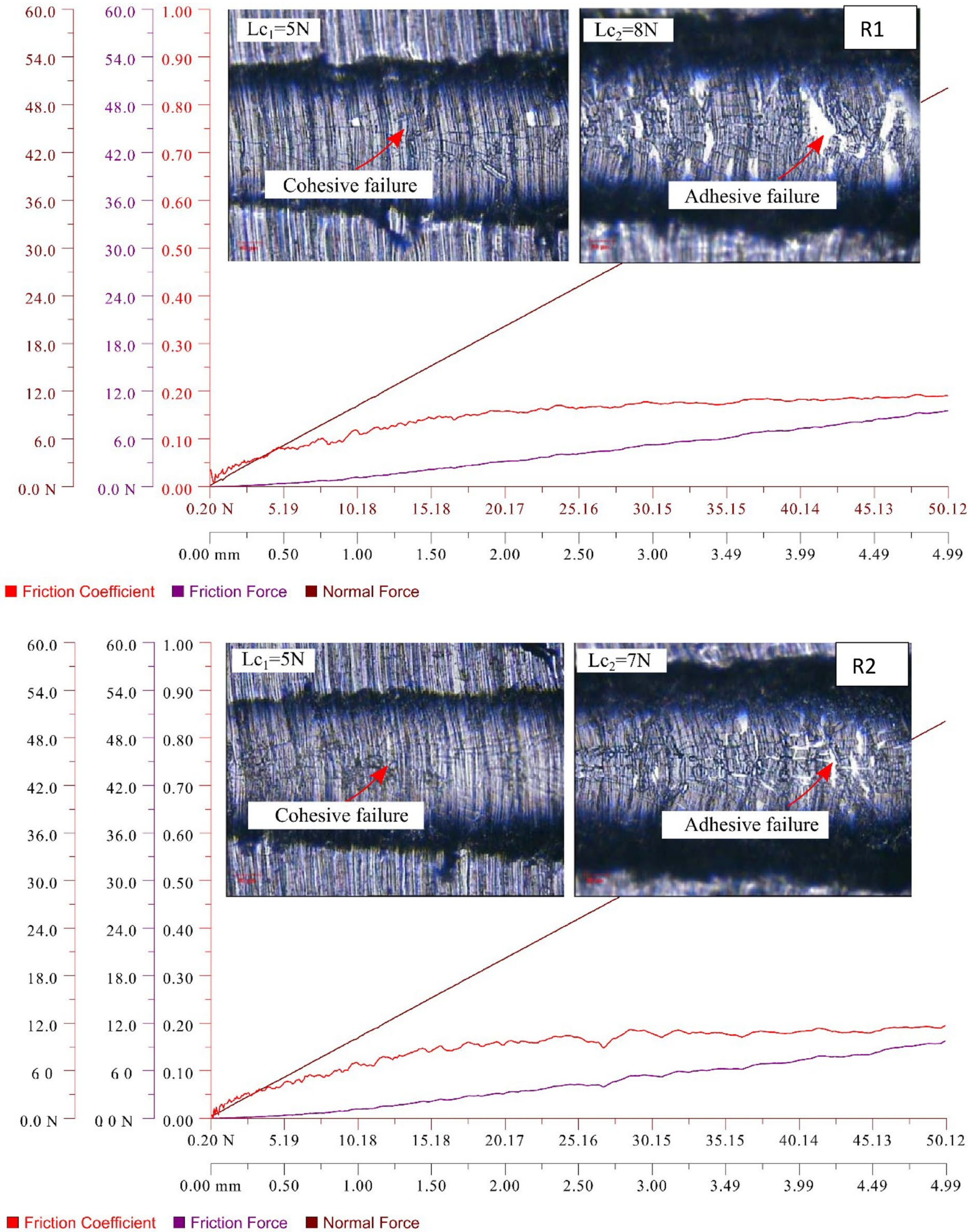

Fig. 10 Scratch test graph of CrAlYN/CrYN gradient coatings grown by HiPIMS-PVD method on AZ91 alloy under R1-R4 experimental conditions

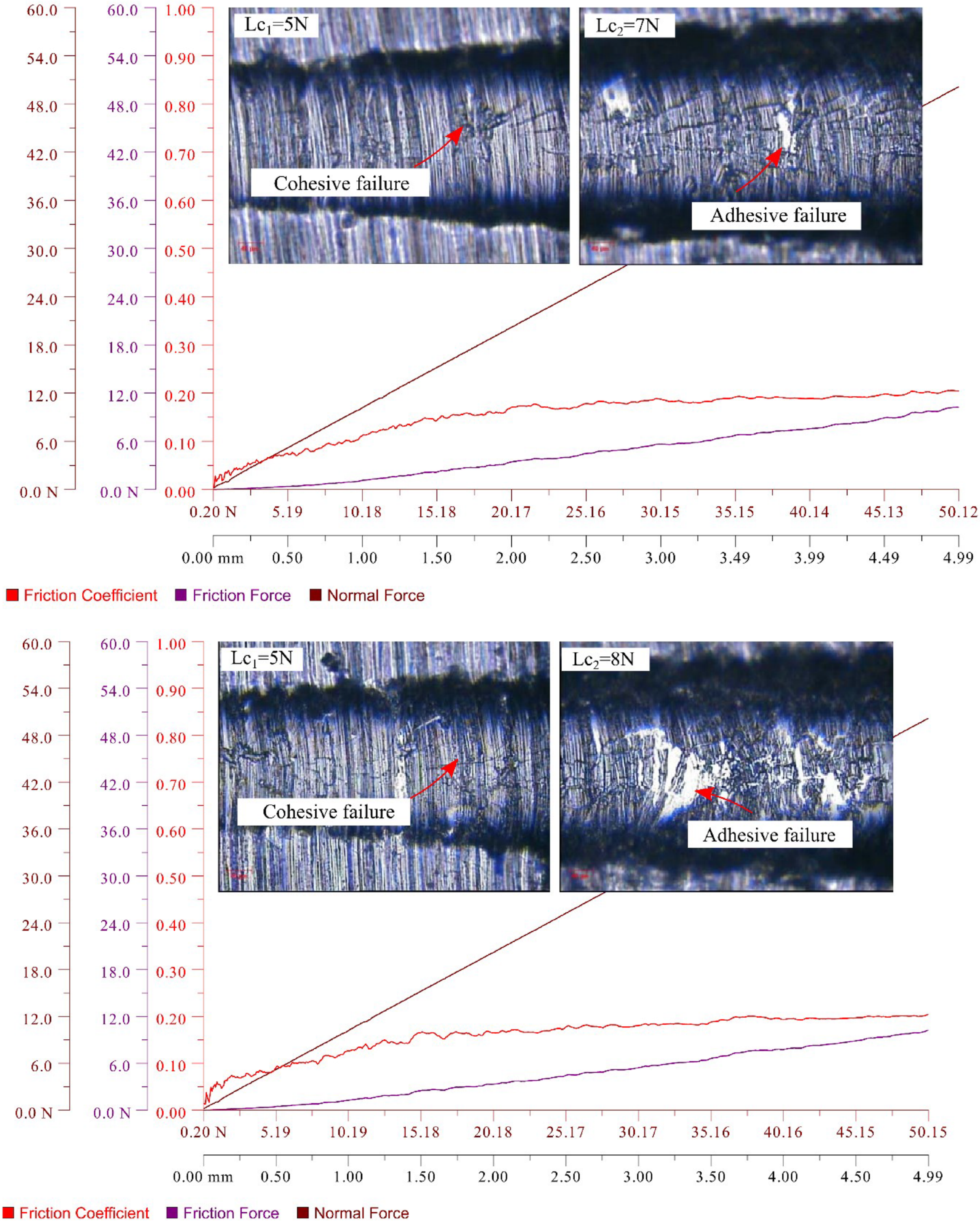

Fig. 10 (continued)

excessive nitrogen penetrates the CrN cages and reduces the soluble amount of AlN. If there is an excessive amount of Cr, Cr is not included in the CrN content. The results obtained are consistent with those reported in the literature.

Figure 14 shows the scratch test results for AZ91 base materials of duplex coatings enlarged at different parameters and levels according to the Taguchi L4 experimental plan. During the process, Lc2 values were considered as

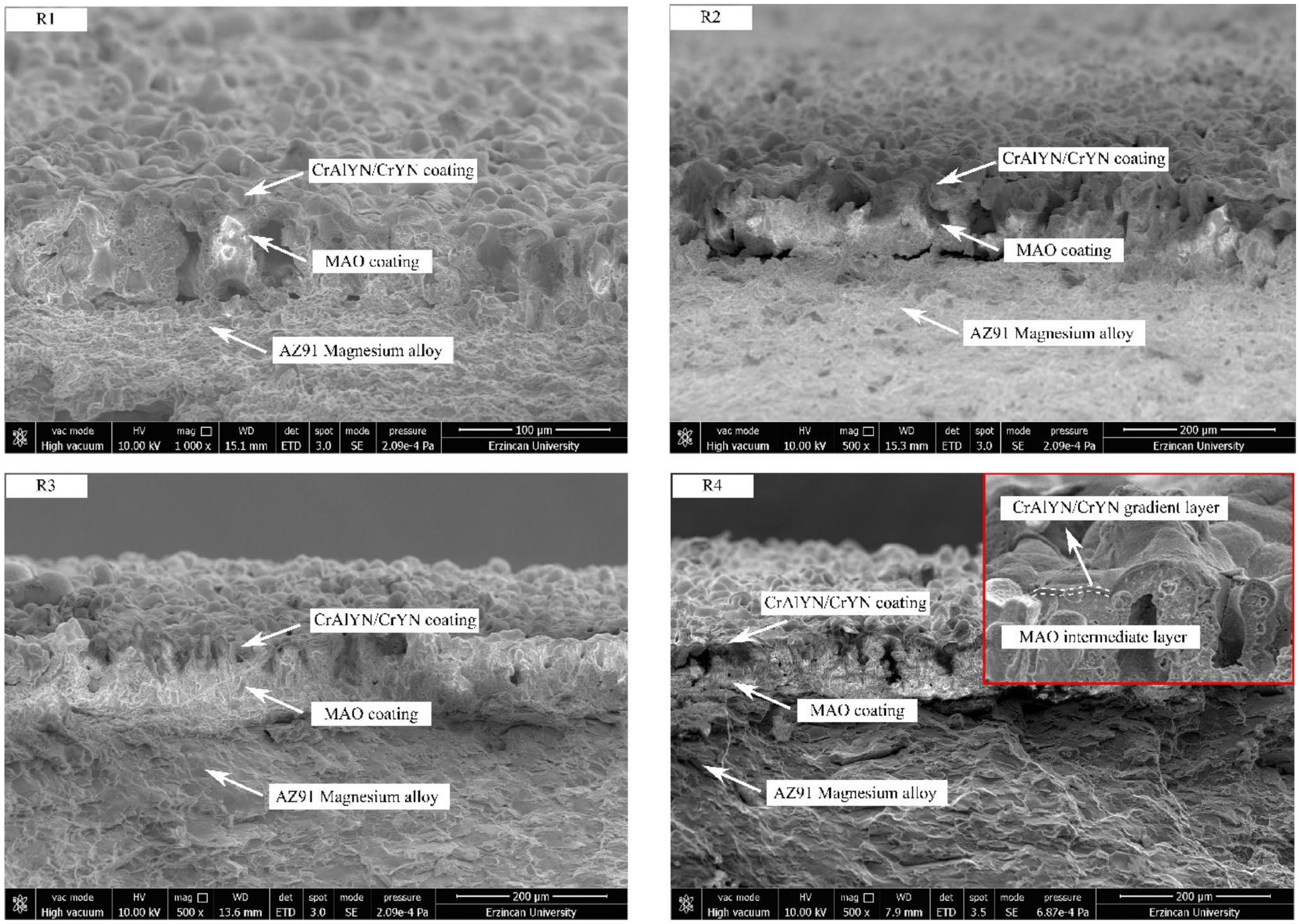

Fig. 11 The cross-sectional view of duplex coatings grown on AZ91 alloy under R1-R4 experimantal conditions

they relate to the adhesion force that damages duplex coatings. Figure 14 shows the numerical values of the critical load force (Lc2) of the enlarged duplex coatings on AZ91 base materials. In the R1 and R2 experimental conditions, a scratch test was performed under increasing loads, starting from 0.2 N and reaching a maximum of 130 N (see Fig. 14). In the R3 and R4 conditions, a scratch test was conducted up to a maximum load of 120 N.

Examining the scratch test graphs revealed that the highest Lc2 critical load value between the duplex coatings on the AZ91 alloy occurred in the R1 conditions (Lc2 $\simeq$ 110 N). Examining the parameter levels in the R1 test conditions revealed that the lowest voltage (400 V) was applied to the CrY target, the lowest current (0.5 A) to the Al target, and the lowest amount of N_2 (2.5 g) to the system (as seen in Table 4 and 5). In the R1 conditions, Lc1 values indicating cohesive strength were found to be approximately 70 N; however, cracks were observed on the edges of the scratch trail of four different duplex coatings when the scratch test images were examined. These cracks are thought to be caused by stress. These cracks, which are circular and quite small within the scratch trail, can be considered as conformal cracks [32].

These cracks, which were both conformal and under stress, enlarged with an increase in load. This caused the AZ91 base material coating layer to separate from the base material, resulting in flaking on the trail edges. Examining the coating thickness revealed that it had the lowest value (t $\simeq$ 0.83 µm) in the R1 experimental conditions where adhesive strength was obtained (Fig. 14). This study concluded that adhesion increased by approximately 4.5 times more than with CrAlYN/CrYN gradient coatings directly applied to an AZ91 base material.

After the MAO process, CrAlYN/CrYN was coated and the AZ91 alloy's scratch test results were obtained using the Taguchi experimental design method. It is well known that mechanical incompatibility between the base material and the coating is an important obstacle, since the elasticity modulus and hardness of hard coatings on magnesium and its alloys are lower. In recent years, various surface improvement techniques have been developed to eliminate this incompatibility. One of these techniques is the duplex coating method. To remove the mechanical incompatibility between the CrAlYN/CrYN gradient coatings and the base material, an MgO layer was enlarged using the MAO

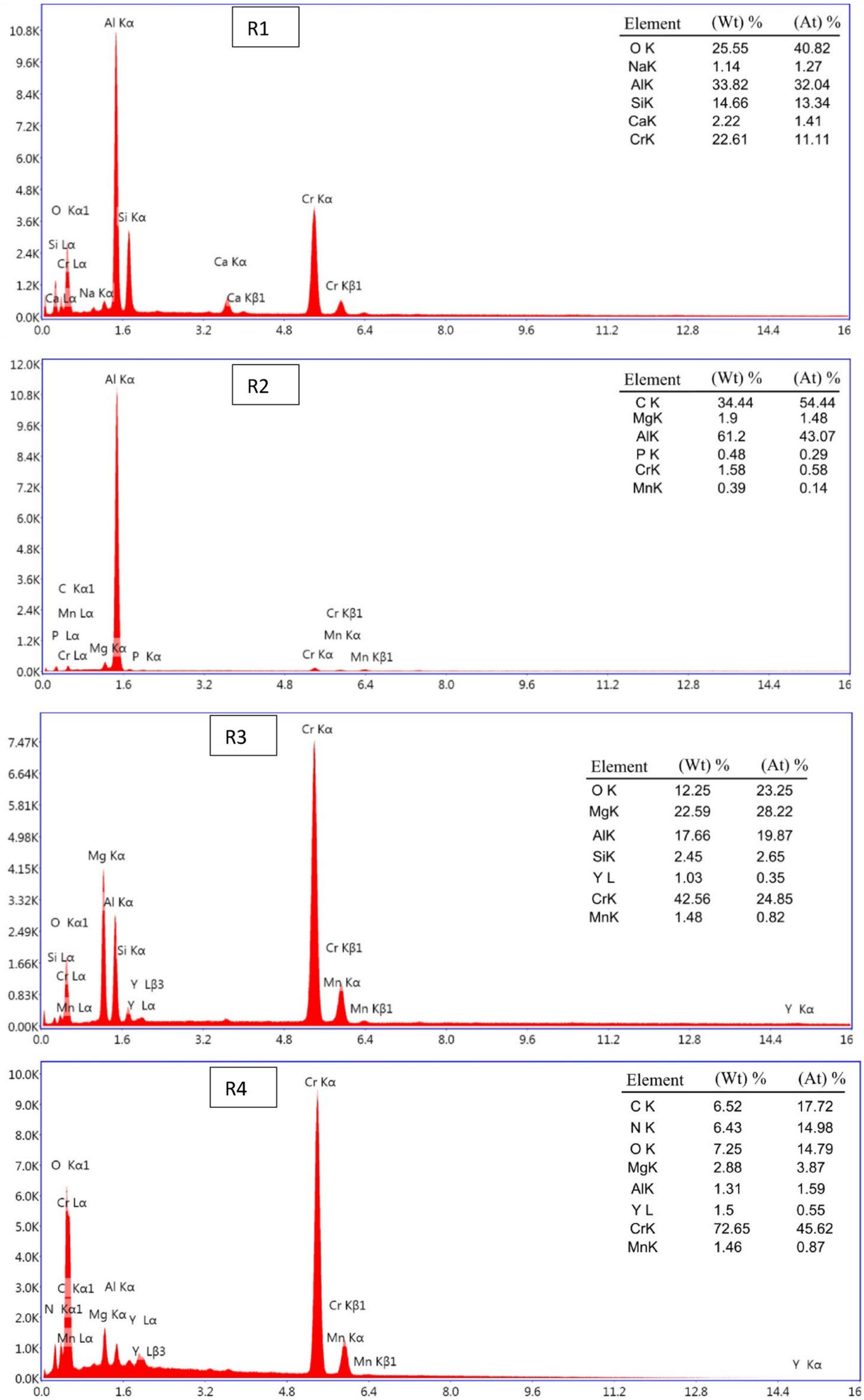

Fig. 12 EDS analysis of duplex coatings grown on an AZ91 alloy under R1-R4 experimental conditions

method on the AZ91 magnesium alloy. The MgO layer formed during the MAO process, which was optimised in terms of adhesion properties on AZ91 base materials, was applied to the base materials as an intermediate layer. The CrAlYN/CrYN gradient coatings formed on the intermediate layer were analysed using the ANOVA-TM package programme after scratch tests on the duplex coatings were performed to optimise the adhesion properties of the gradient coatings. 'Larger is better' performance statistics were selected as the optimisation criterion.

To identify the effects of the parameters on the optimisation criterion, a review of the relevant literature was

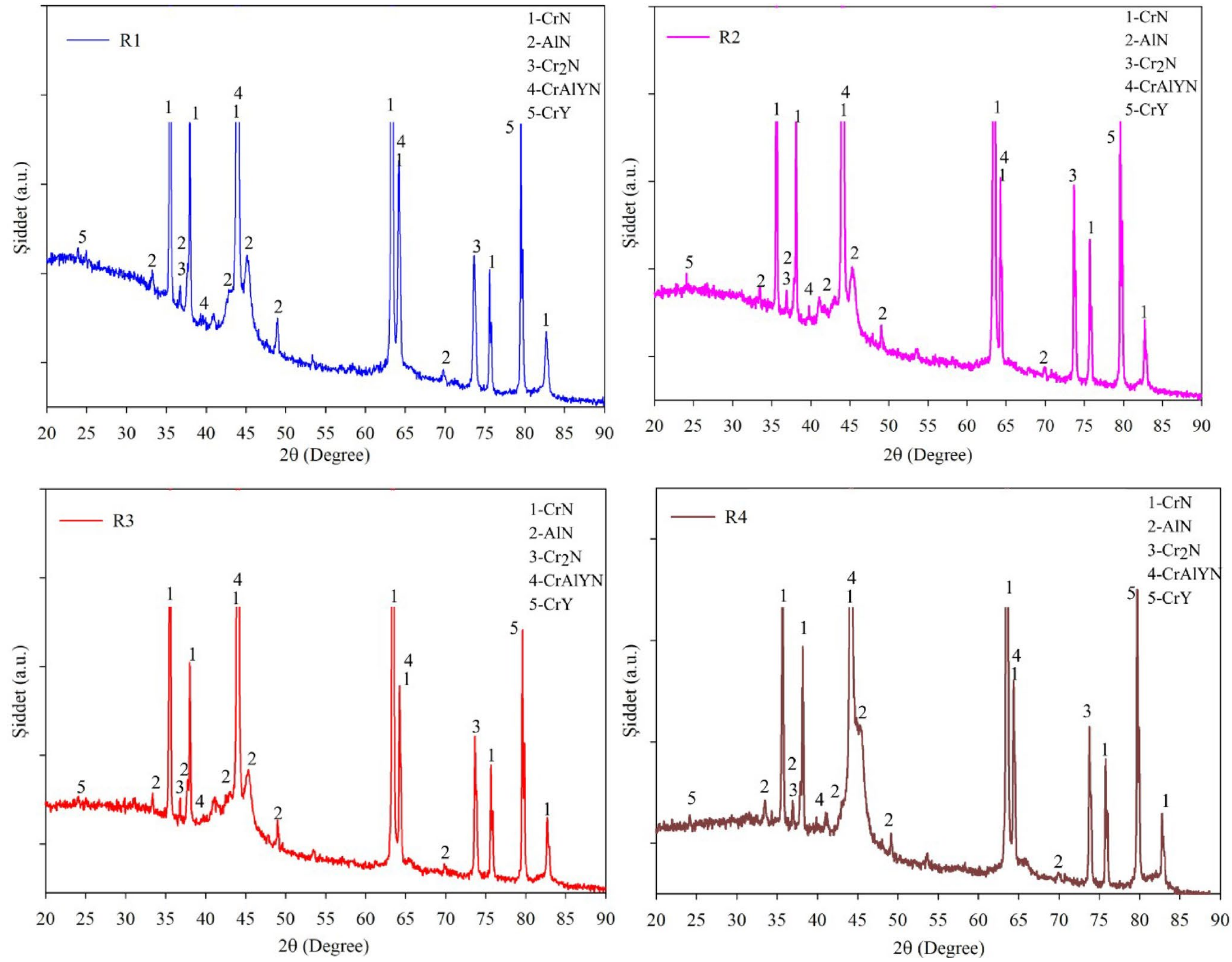

Fig. 13 XRD analysis of duplex coatings grown on an AZ91 alloy under R1 test conditions

conducted. According to the results of the scratch test, the Lc2 value was considered a critical load in the adhesion tests of the coatings. For the Lc2 critical load value, 'larger is better' statistics were used. The objective of this process was to determine the optimal Lc2 value under the experimental conditions. The effect of each parameter on the optimisation criterion was calculated, and the performance statistics graph is presented in Fig. 15. The optimisation process has been completed, meaning that the numerical value of the maximum points in the graph shows the optimum value of the relevant parameter, while the numerical value of the minimum points shows the worst value according to 'larger is better' performance statistics.

The values shown in Table 8 are the outputs of the ANOVA-TM program. It was found that the most effective parameter for duplex coatings was the 'voltage value to CrY target'. Table 9 shows the statistical values of the data obtained under the R1, R2, R3 and R4 experimental conditions using the ANOVA-TM package program. When the adhesion of the duplex coatings to the AZ91 base material was evaluated, it was found that the most effective parameters for achieving the highest critical load (Lc2) were the voltage applied to the CrY target, the current applied to the Al target, and the amount of N_2 used during coating, respectively.

The confidence interval was evaluated for the difference between the estimated and found values. Here, the estimated error is the relationship between the theoretical experimental conditions, the application of the verification experiment, and the values found. The confidence interval for the estimated error was calculated using the ANOVA-TM package program. The adhesion properties optimised using the Taguchi experimental design method were found to lie within the 95% confidence interval. As the performance values obtained in the verification experiments fall within the calculated confidence interval, the experimental results can be considered acceptable at a 5% error level. This process is consistent with the literature [32].

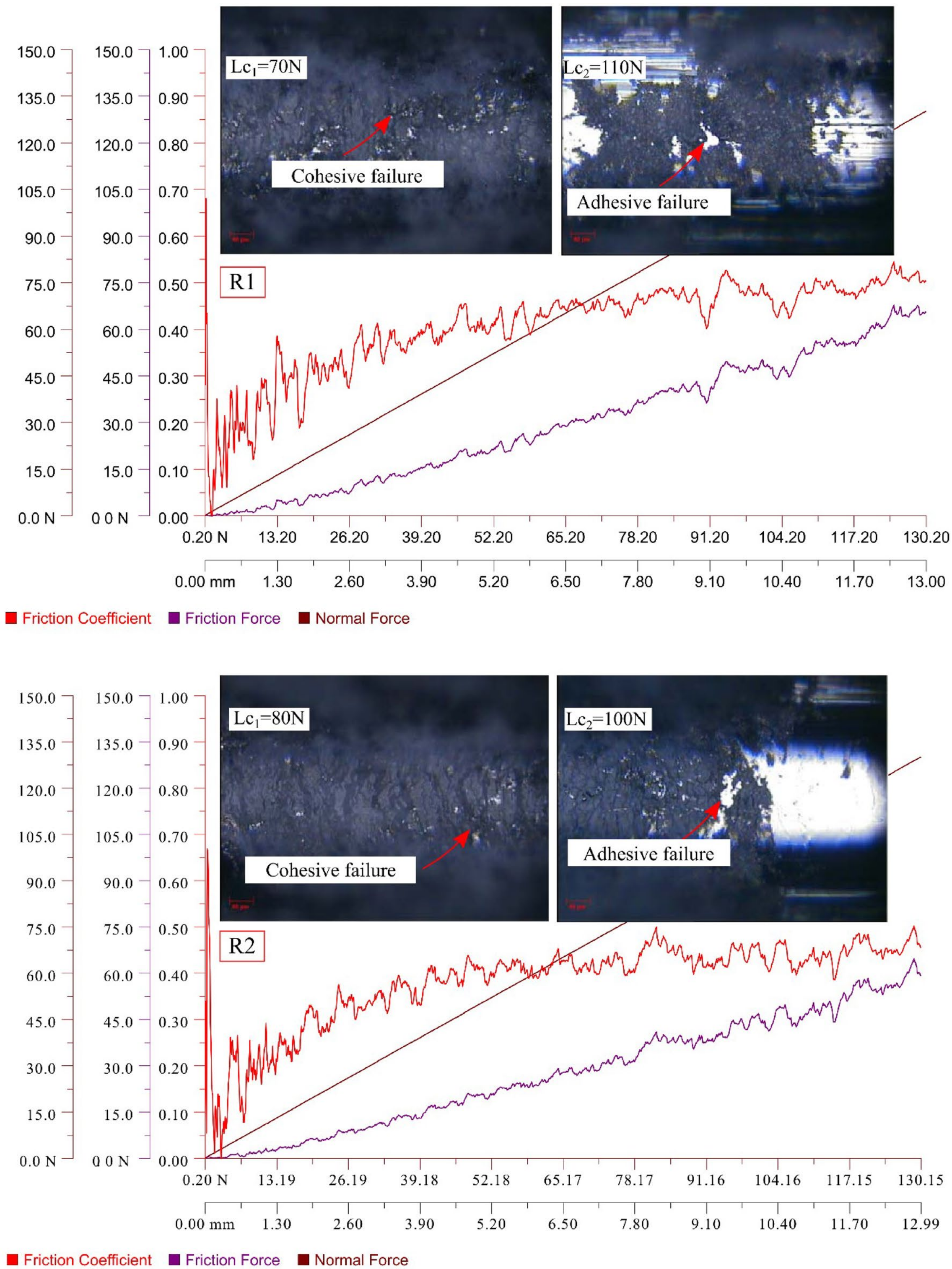

Fig. 14 Scratch test plot of duplex coatings grown on an AZ91 alloy under R1-R4 test conditions

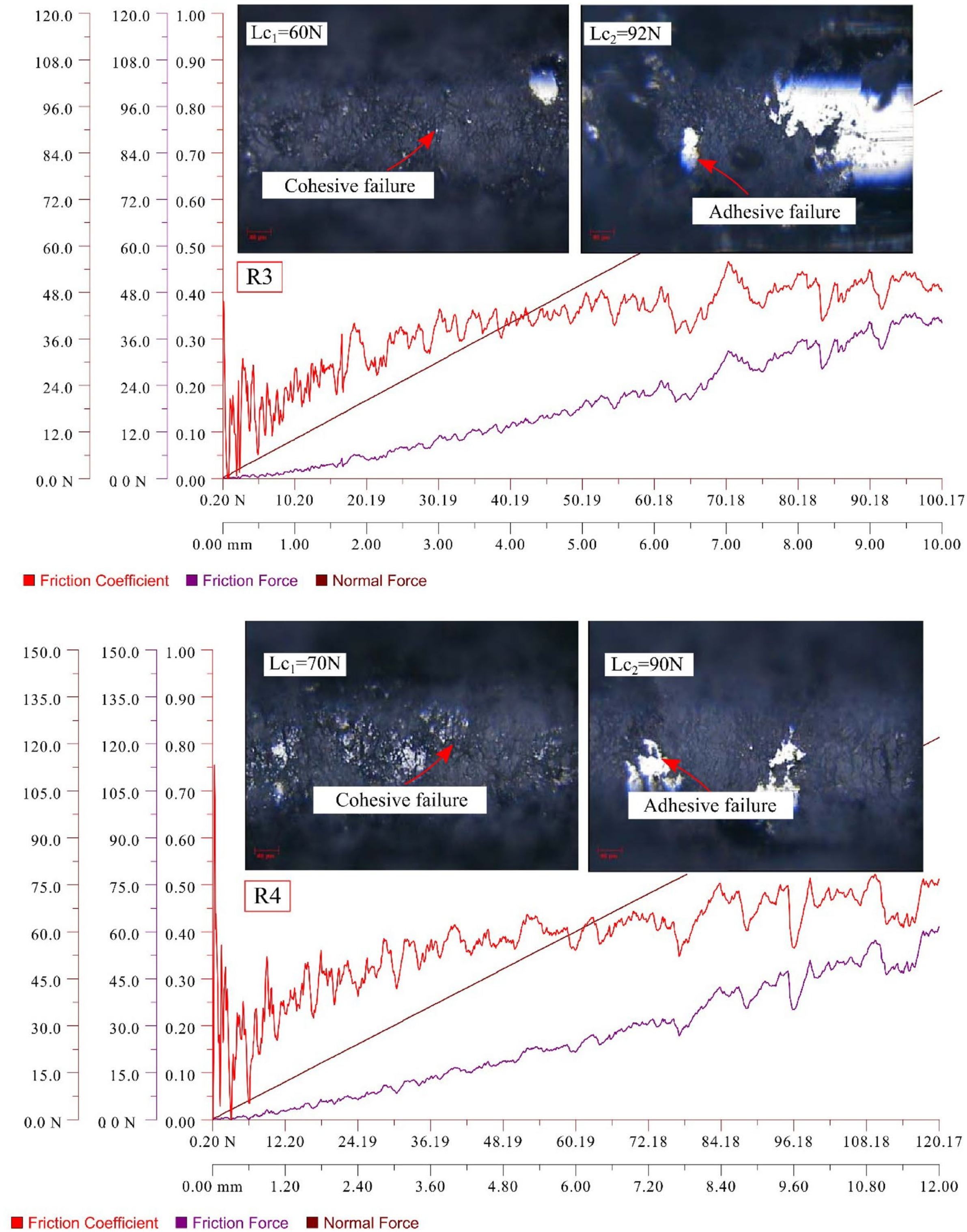

Fig. 14 (continued)

Conclusions

This study examined the structural properties of duplex-coated AZ91 alloy, the effects of changing the process parameters on the structure of the coatings, and the adhesion behaviour of the coatings enlarged with the base material, using MAO and HiPIMS-PVD methods. The results obtained in the study are presented below:

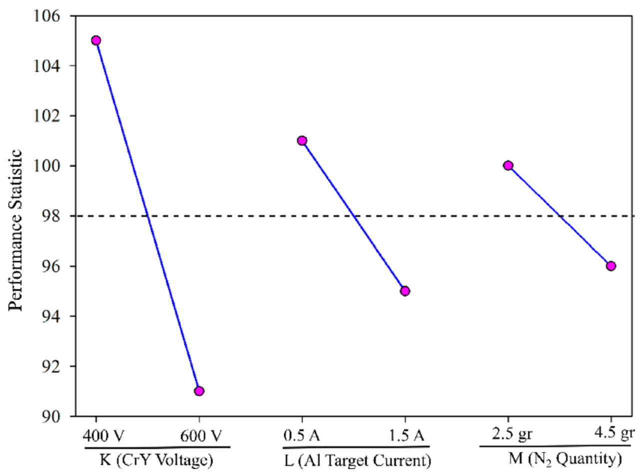

Fig. 15 Performance statistics graph affecting the adhesion of duplex coatings grown on an AZ91 alloy

Table 8 Order of influence of parameters on adhesion properties

	K	L	M
Level 1	105.000	101.0000	100.000
Level 2	91.0000	95.0000	96.0000
Delta	14.0000	6.0000	4.0000
Rank	1	2	3

Micro Arc Oxidation

- Depending on the micro-discharge incident caused by the MAO method, it was observed that the AZ91 coatings had rough surfaces, micro-gaps of various sizes (pores) and volcanic structures. It was also found that the dimensions of the microporosity and their distribution on the surface changed depending on the coating parameters and their respective values. In experiment 1, with one parameter (700 Hz, 500 V and Type A solution), there were fewer micro gaps and they were smaller in diameter.
- In the coatings that were enlarged as a result of XRD analyses at 2θ levels of 36.39°, 38.02°, 42.98°, 62.36° and 74.71°, the presence of MgO phases was found to be more intense in experiments 1 and 4 than in the other experimental conditions. The basic phase in the coating structure was MgO, but the Mg_2SiO_4 and $Mg(PO_4)$ phases formed as a result of the chemicals in the $Na_2SiO_3.5H_2O$, Na_2HPO_4 and KOH aqueous solution.
- It was also observed that coating thicknesses changed depending on the level values of the coating parameters enlarged on the AZ91 alloy. The lowest average coating thickness obtained was 26 µm in Experiment 1 conditions, while the highest was 60 µm in Experiment 2 conditions.
- When evaluating the adhesion of the enlarged MgO coatings to the base materials, the parameters that were most effective in achieving the largest critical load value (Lc2) were found to be voltage, solution type and frequency. According to the performance statistics of the Taguchi test design, the greatest value was found to be a frequency of 700 Hz, a Type B solution (3 g/l) and a voltage of 650 V (experiment 2).
- As a result of the verification experiments conducted according to the levels of the parameters determined by optimisation, the critical load value was found to be $L_c2 = 24$ N.
- When the surface roughness values obtained from the surfaces of the enlarged MgO coatings were evaluated, the lowest values were found to be Ra ≈ 1.53 µm and Rz ≈ 11.4 µm under experiment 3 conditions, while the highest values were found to be Ra ≈ 4.34 µm and Rz ≈ 27.8 µm under experiment 2 conditions.

CrAlYN/CrYN Gradient Coating;

- According to the measurements, the lowest coating thickness was obtained in R1 test conditions at t ≃ 0.83 µm, while the highest coating thickness was obtained in R2 test conditions at t ≃ 1.66 µm.
- The coatings obtained in all experimental conditions had a very dense, homogeneous, smooth and compact microstructure.
- According to EDS analyses taken from the surface of CrAlYN/CrYN gradient coatings in R2 experimental conditions, it was found that the aluminium content was higher than in the other conditions, as was the current value applied to the Al target. It is thought that this condition also increases the coating thickness.

Table 9 Statistical data of the ANOVA-TM package program

Experiment No	Data	Total	Mean	S(squares)	S(squares)	Variation	S(squares)	Variance
	n	t	m	Ss	Sr	St	Sm	Ve
1	1	110.0000	110.0000	12,100.000	0.0001	0.0000	12,100.000	0.0000
2	1	100.0000	100.0000	10,000.000	0.0001	0.0000	10,000.000	0.0000
3	1	92.0000	92.0000	8,464.0000	0.0001	0.0000	8,464.0000	0.0000
4	1	90.0000	90.0000	8,100.0000	0.0001	0.0000	8,100.0000	0.0000
All data	**N**	**T**	**M**	**SS**	**SR**	**ST**	**SM**	**VE**
	4	392.0000	98.0000	38,664.000	0.0004	248.0000	38,664.00	82.6667

- CrN, AlN and Cr_2N phases were observed in the structure of the coatings, which were enlarged as a result of XRD analyses. The presence of CrN and AlN phases at $2\theta \simeq 37°$ and $2\theta \simeq 44°$ was found to be very high in the R1, R2 and R4 experimental conditions compared to R3.
- When the adhesion of the enlarged CrAlYN/CrYN gradient coatings to the base materials was evaluated, it was found that the values ranged between 0 and 5 N for all experimental conditions, indicating cohesive strength. The Lc_2 values indicating adhesive strength ranged between 5 and 10 N. These results suggest that the adhesion strength between the enlarged CrAlYN/CrYN gradient coatings and the AZ91 alloy base material is very low.

Duplex Coating (CrAlYN/CrYN on MgO Intermediate Layer)

- According to the measurements, the highest coating thickness was obtained in R2 experimental conditions, with CrAlYN/CrYN gradient coatings enlarged on the base material. According to the R2 test conditions, the highest thickness was detected at the levels at which voltage was applied to the CrY target material. Of the parameters affecting duplex coatings, the current value applied to the Al target was 1.5 A, and 4.5 g of N_2 was given to the system.
- Based on SEM images, it was found that a prominent line was formed where the MAO oxide layer separated from the base materials. CrAlYN/CrYN gradient coatings grown on this layer under four different coating conditions exhibited a columnar structure with a very dense, homogeneous, smooth and compact microstructure.
- XRD analysis showed that the coatings contained CrN, AlN, Cr_2N, CrAlN and CrY. The CrN intensity was found to be particularly high in the R1, R2, R3 and R4 experimental conditions.
- When the adhesion of duplex coatings on AZ91 alloy base materials was evaluated, the values ranged between 60 and 80 N for all experimental conditions, indicating cohesive strength. The Lc2 values expressing adhesive strength ranged between 90 and 110 N, with the highest value (Lc2 $\simeq$ 110 N) occurring in R1 test conditions. This value occurred at the lowest applied voltage to the CrY target (400 V), the lowest current applied to the Al target (0.5 A), and the lowest amount of N_2 introduced to the system (2.5 g).
- It was concluded in the study that, when the adhesion of duplex coatings was evaluated against the base material, the adhesion increased four-and-a-half-fold. CrAlYN/CrYN gradient coatings were found to enlarge directly on the AZ91 base material.

Acknowledgements We would like to thank the Gümüşhane University BAP Coordination Unit (GÜBAP) for supporting our project numbered 21.E3103.07.01 and 18.F5111.02.01 with GÜBAP2907.

Author contributions All have done equal contribution.

Funding There is no funding declaration.

Data availability The datasets generated during and/or analyzed during the current study are available from the corresponding author on reasonable request.

Declarations

Ethical approval The manuscript has not been submitted to any journal for simultaneous review. The submitted work is original. This article complies with the ethical standards of the journal.

Competing interests There is no conflict of interest by any form for this manuscript.

References

1. Chen, X.B., Easton, M.A., Birbilis, N., Yang, H.Y., Abbott, T.B.: Corrosion-resistant coatings for magnesium (Mg) alloys, corrosion prevention of magnesium. In: Alloy, L.G., Song (eds.) Woodhead Publishing, pp. 282–312. CRC, Oxford (2013). https://doi.org/10.1533/9780857098962.2.282
2. Dong, H.: Surface Engineering of Light Alloys: Aluminium, Magnesium and Titanium Alloys, p. 640. Woodhead Publishing in Materials, CRC, Oxford (2010)
3. Song, G.L.: In: Song, G.L., Publishing, W. (eds.) Corrosion Behavior and Prevention Strategies for Magnesium (Mg) Alloys, Corrosion Prevention of Magnesium Alloy, pp. 3–37. CRC, Oxford (2013). https://doi.org/10.1533/9780857098962.1.3
4. Sun, Y., Wang, R., Peng, C., Feng, Y., Yang, M.: Corrosion behavior and surface treatment of superlight Mg – Li alloys. Trans. Nonferrous Met. Soc. China. **27**, 1455–1475 (2017). https://doi.org/10.1016/S1003-6326(17)60167-5
5. Rams, J., Torres, B., Pulido-González, N., García-Rodriguez, S., Alloys, M.: Fundamentals and Recent Advances, Encyclopedia of Materials: Metals and Alloys, 1 pp. 2–10. (2022). https://doi.org/10.1016/B978-0-12-819726-4.00082-X
6. Zarka, M., Dikici, B., Niinomi, M., Ezirmik, K.V., Nakai, M., Yilmazer, H.: A systematic study of β-type Ti-based PVD coatings on magnesium for biomedical application. Vacuum. **183**, 109850 (2021). https://doi.org/10.1016/j.vacuum.2020.109850
7. Çelik, A., Bozkurt, Y.B.: Improvement of tribological performance of AZ31 biodegradable alloy by TiN-based PVD coatings. Tribol. Int. **173**, 107684 (2022). https://doi.org/10.1016/j.triboint.2022.107684
8. Sukuroglu, S., Sukuroglu, E.E., Totik, Y., Gulten, G., Efeoglu, I., Avci, S.: Corrosion and adhesion properties of MAO-coated LA91 magnesium alloy. Mater. Sci. Technol. **40**, 616–632 (2024). https://doi.org/10.1177/02670836231219868
9. Kumaradhas, P., Sivapragash, M.: Comparison of corrosion behaviour of heat treated, ZrO2 and ZrN PVD coated AZ91D Mg alloy, Materials Today: Proceedings, 56 Part 1 pp. 527–532. (2022). https://doi.org/10.1016/j.matpr.2022.02.181
10. Aktug, S.L., Durdu, S., Aktas, S., Yalcin, E., Usta, M.: Surface and in vitro properties of Ag-deposited antibacterial and bioactive

coatings on AZ31 Mg alloy. Surf. Coat. Technol. **375**, 46–53 (2019). https://doi.org/10.1016/j.surfcoat.2019.07.013
11. Westengen, H., Rashed, H.M.M.A.: Magnesium Alloys: Properties and Applications, Encyclopedia of Materials: Metals and Alloys, 1 pp.11–19. (2016). https://doi.org/10.1016/B978-0-12-803581-8.02568-6
12. Qin, B., Zhou, S., Chen, H., Wang, M.: Superior corrosion and wear resistance of AZ91D Mg alloy via electrodeposited SiO2–Ni-based composite coating. Mater. Chem. Phys. **283**, 126001 (2022). https://doi.org/10.1016/j.matchemphys.2022.126001
13. Chengtong, Y., Lina, J., Gaoxiang, X., Fangfang, W., Xinchao, W., Hu, Z.: Microstructure and initial corrosion behavior of double-layer Zn-Al-Mg coatings produced by PVD. Surf. Coat. Technol. **366**, 214–226 (2019). https://doi.org/10.1016/j.surfcoat.2019.03.029
14. Sukuroglu, E.E., Totik, Y., Arslan, E., Efeoglu, I.: Analysis of Tribo-corrosion Properties of MAO/DLC Coatings Using a Duplex Process on Ti6Al4V Alloys. J Bio Tribo Corros. **1**, 22 (2015). https://doi.org/10.1007/s40735-015-0022-z
15. Aliofkhazraei, M., Ali, N.: PVD technology in fabrication of Micro- and nanostructured coatings. Compr. Mater. Process. **7**, 49–84 (2014). https://doi.org/10.1016/B978-0-08-096532-1.00705-6
16. Zhang, Y., Chen, F., Zhang, Y., Liu, M., Pang, Y., Du, C.: Enhanced corrosion and tribocorrosion properties of duplex TiN-MAO coating prepared on TC17 alloys. Surf. Coat. Technol. **444**, 128662 (2022). https://doi.org/10.1016/j.surfcoat.2022.128662
17. Wang, Z., Xu, B., Chen, Y., Bao, F., Liu, Y., Jiang, W., Xing, Z.: Amorphous/nanocrystalline HEA films on MAO surfaces: Gradient structure design and tribological performance optimization. Surf. Coat. Technol. 132298 (2025). https://doi.org/10.1016/j.surfcoat.2025.132298
18. Li, H., Wang, Q., Zhuang, M., Wu, J.: Characterization and residual stress analysis of tin/ticn films on AZ31 magnesium alloy by PVD. Vacuum. **112**, 66–69 (2015). https://doi.org/10.1016/j.vacuum.2014.11.019
19. Adesina, A.Y., Gasem, Z.M., Mohammed, A.S.: Comparative investigation and characterization of the scratch and wear resistance behavior of tin, crn, AlTiN and AlCrN cathodic Arc PVD coatings. Arab. J. Sci. Eng. **44**, 10355–10371 (2019). https://doi.org/10.1007/s13369-019-04038-8
20. Liu, F., Han, Y., Guo, X., Wang, C., Zhang, K.: Adhesion and machining performance of PVD AlCrN coatings with an ion beam/laser textured substrate. Surf. Coat. Technol. **423**, 127607 (2021). https://doi.org/10.1016/j.surfcoat.2021.127607
21. Sivapragash, M., Kumaradhas, P., Retnam, B.S.J., Joseph, X.F., Pillai, U.T.S.: Taguchi based genetic approach for optimizing the PVD process parameter for coating ZrN on AZ91D magnesium alloy. Mater. Design. **90**, 713–722 (2016). https://doi.org/10.1016/j.matdes.2015.11.027
22. Zhong, Z., Zhang, L., Chen, Y., Gu, J., Zhu, J., Xiong, X.: Strategy for achieving high-performance PVD nano-multilayered altin/tin coated milling tool: Fine platelet-grained WC–Co substrate and interface regulation. Surf. Coat. Technol. **435**, 128265 (2022). https://doi.org/10.1016/j.surfcoat.2022.128265
23. Sivapragash, M., Kumaradhas, P., Vettivel, S.C., Retnam, B.S.J.: Optimization of PVD process parameter for coating AZ91D magnesium alloy by Taguchi grey approach. J. Magnesium Alloys. **6**, 2 (2018). https://doi.org/10.1016/j.jma.2018.02.004
24. Arslan, E., Totik, Y., Demirci, E.E., Efeoglu, I.: Wear and adhesion resistance of duplex coatings deposited on Ti6Al4V alloy using MAO and CFUBMS, surface and coatings technology, **214** pp. 1–7. (2013). https://doi.org/10.1016/j.surfcoat.2012.10.006
25. Hoche, H., Groß, S., Oechsner, M.: Development of new PVD coatings for magnesium alloys with improved corrosion properties. Surf. Coat. Technol. **259**(Part A), 102–108 (2014). https://doi.org/10.1016/j.surfcoat.2014.04.038
26. Haneef, M., Evaristo, M., Morina, A., Yang, L., Trindade, B.: New nanoscale multilayer Magnetron sputtered Ti-DLC/DLC coatings with improved mechanical properties. Surf. Coat. Technol. **480**, 130595 (2024). https://doi.org/10.1016/j.surfcoat.2024.130595
27. Sukuroglu, S.: Characterization, corrosion, adhesion and wear properties of al2O3 and al2O3:TiB2 composite coating on al 7075 aluminum alloy by one-step micro-arc oxidation method. Mater. Today Commun. **46**, 112493 (2025). https://doi.org/10.1016/j.mtcomm.2025.112493
28. Yeşildal, R., Karabudak, F., Şüküroğlu, E.E., Şüküroğlu, S., Zamanlou, H., Bayındır, F., Şen, S., Totik, Y.: Differential scanning calorimetry (DSC) and Ni + 2 release analysis of NiTi-shape-memory dental alloys coated by micro-arc oxidation (MAO) method. Appl. Phys. A. **124**, 572 (2018). https://doi.org/10.1007/s00339-018-1973-y
29. Sukuroglu, E.E.: Investigation of antibacterial susceptibility of Ag-doped oxide coatings onto AZ91 magnesium alloy by micro-arc oxidation method, Adv. Mater. Sci. Eng., pp. 1–7. (2018). (2018) https://doi.org/10.1155/2018/6871241
30. Wu, G., Zhu, L., Chen, X., Li, L., Zhang, S., Wang, Y., Wen, C., Yao, J.: Growth characteristics and wear properties of micro-arc oxidation coating on Ti-6Al-4V with different laser texture shapes. Surf. Coat. Technol. **475**, 130108 (2023). https://doi.org/10.1016/j.surfcoat.2023.130108
31. Ko, Y.G., Namgung, S., Shin, D.H.: Correlation between KOH concentration and surface properties of AZ91 magnesium alloy coated by plasma electrolytic oxidation. Surf. Coat. Technol. **205**, 7 (2010). https://doi.org/10.1016/j.surfcoat.2010.09.055
32. Demirci, E.E., Arslan, E., Ezirmik, K.V., Baran, Ö., Totik, Y., Efeoğlu, İ.: Investigation of wear corrosion and tribocorrosion properties of AZ91 Mg alloy coated by micro Arc oxidation process in the different electrolyte solutions. Thin Solid Films. **528**, 15 (2013). https://doi.org/10.1016/j.tsf.2012.07.145
33. Darband, G.B., Aliofkhazraei, M., Hamghalam, P., Valizade, N.: Plasma electrolytic oxidation of magnesium and its alloys: Mechanism, properties and applications. J. Magnesium Alloys. **5**, 1 (2017). https://doi.org/10.1016/j.jma.2017.02.004
34. Zhang, S.F., Zhang, R.F., Li, W.K., Li, M.S., Yang, G.L.: Effects of Tannic acid on properties of anodic coatings obtained by micro Arc oxidation on AZ91 magnesium alloy. Surf. Coat. Technol. **207**, 170–176 (2012). https://doi.org/10.1016/j.surfcoat.2012.06.056
35. Liu, S., Yang, Y., Lan Ng, F., Ji, R., Zeng, X.T.: Oxidation behaviour of CrAlYN coatings at elevated temperatures. Surf. Coat. Technol. **320**, 357–361 (2017). https://doi.org/10.1016/j.surfcoat.2016.12.030
36. Hussein, R.O., Northwood, D.O., Nie, X.: The effect of processing parameters and substrate composition on the corrosion resistance of plasma electrolytic oxidation (PEO) coated magnesium alloys. Surf. Coat. Technol. **237**, 357–368 (2013). https://doi.org/10.1016/j.surfcoat.2013.09.021
37. Lv, G.H., Chen, H., Gu, W.C., Li, L., Niu, E.W., Zhang, X.H., Yang, S.Z.: Effects of currents frequency on the structural characteristics and corrosion property of ceramic coatings formed on magnesium alloy by PEO technology. J. Mater. Process. Technol. **208**, 1–3 (2008). https://doi.org/10.1016/j.jmatprotec.2007.12.125
38. Yang, Y., Wu, H.: Effects of current frequency on the microstructure and wear resistance of ceranic coatings embedded with SiC Nano-Particles produced by Micro-Arc oxidation on AZ91D magnesium alloy. J. Mater. Science&Technology. **26**, 10 (2010). https://doi.org/10.1016/S1005-0302(10)60138-7

39. Martin, J., Nomine, A.V., Stef, J., Nomine, A., Zou, J.X., Henrion, G., Grosdidier, T.: The influence of metallurgical state of substrate on the efficiency of plasma electrolytic oxidation (PEO) process on magnesium alloy. Mater. Desing. **178**, 107859 (2019). https://doi.org/10.1016/j.matdes.2019.107859
40. Bayati, M.R., Zargar, H.R., Talimian, A., Ziaee, A., Molaei, R.: Characterization of Al2O3-TiO2 nano porous solar absorbers derived via MAO/Sol-Gel hybrid process. Surf. Coat. Technol. **205**(7), 2483–2489 (2010). https://doi.org/10.1016/j.surfcoat.2010.09.046
41. Bai, A., Chen, Z.J.: Effect of electrolyte additives on Anti-Corrosion ability of Micro-Arc oxide coatings formed on magnesium alloy AZ91D. Surf. Coat. Technol. **203**(14), 1956–1963 (2009). https://doi.org/10.1016/j.surfcoat.2009.01.032
42. Chen, X., Ou, J., Wei, Y., Huang, Z., Kang, Y., Yin, G.: Effect of MgO contents on the mechanical properties and biological performances of bioceramics in the MgO-CaO-SiO2 system. J. Mater. Sci: Mater. Med. **21**, 1463–1471 (2010). https://doi.org/10.1007/s10856-010-4025-5
43. Durdu, S., Aytaç, A., Usta, M.: Characterization and corrosion behavior of ceramic coating on magnesium by Micro-Arc oxidation. J. Alloys Compd. **509**, 34 (2011). https://doi.org/10.1016/j.jallcom.2011.06.059
44. Jia, X., Song, J., Zhao, L., Jiang, B., Yang, H., Zhao, T., Zhao, H., Liu, Q., Pan, F.: The corrosion behaviour of MAO coated AZ80 magnesium alloy with surface indentation of different sizes. Eng. Fail. Anal. **136**, 106185 (2022). https://doi.org/10.1016/j.engfailanal.2022.106185
45. Chen, X., Fan, Y.: Study on Preparation, Microstructure and Properties of Micro-Arc Oxidation Ceramic Coating on AZ91 Magnesium Alloy in Phosphate Electrolyte, IOP Conference Series: Materials Science and Engineering, 730 p.012029. (2020). https://doi.org/10.1088/1757-899X/730/1/012029
46. Liang, J., Hu, L., Hao, J.: Characterization of microarc oxidation coatings formed on AM60B magnesium alloy in silicate and phosphate electrolytes. Appl. Surf. Sci. **253**, 4490–4496 (2007). https://doi.org/10.1016/j.apsusc.2006.09.064
47. Akhter, R., Bendavid, A., Munroe, P.: Tailoring the scratch adhesion strength and wear performance of TiNiN nanocomposite coatings by optimising substrate bias voltage during cathodic Arc evaporation. Surf. Coat. Technol. **445**, 128707 (2022). https://doi.org/10.1016/j.surfcoat.2022.128707
48. Aihua, L., Jianxin, D., Haibing, C., Yangyang, C., Jun, Z.: Friction and wear properties of tin, tialn, AlTiN and CrAlN PVD nitride coatings. Int. J. Refract. Met. Hard Mater. **31**, 82–88 (2012). https://doi.org/10.1016/j.ijrmhm.2011.09.010
49. He, Q., DePaiva, J.M., Kohlscheen, J., Beake, B.D., Veldhuis, S.C.: Study of wear performance and tribological characterization of AlTiN PVD coatings with different al/ti ratios during ultra-high speed turning of stainless steel 304. Int. J. Refract. Met. Hard Mater. **96**, 105488 (2021). https://doi.org/10.1016/j.ijrmhm.2021.105488
50. Qi, Z.B., Zhu, F.P., Wu, Z.T., Liu, B., Wang, Z.C., Peng, D.L., Wu, C.H.: Influence of yttrium addition on microstructure and mechanical properties of ZrN coatings. Surf. Coat. Technol. **231**, 102–106 (2013). https://doi.org/10.1016/j.surfcoat.2012.01.056
51. Hovsepian, P.E., Ehiasarian, A.P., Braun, R., Walker, J., Du, H.: Surf. Coat. Technol. **204**, 16–17 (2010). https://doi.org/10.1016/j.surfcoat.2010.02.021 Novel CrAlYN/CrN Nanoscale Multilayer PVD Coatings Produced by the Combined High Power Impulse Magnetron Sputtering/Unbalanced Magnetron Sputtering Technique for Environmental Protection of γ-TiAl Alloys,
52. Ma, D., Harvey, T.J., Wellman, R.G., Ehiasarian, A.P., Hovsepian, P.E., Sugumaran, A.A., Purandare, Y.P., Wood, R.J.K.: Cavitation erosion performance of cralyn/crn nanoscale multilayer coatings deposited on Ti6Al4V by HİPIMS. J. Alloys Compd. **788**, 719–728 (2019). https://doi.org/10.1016/j.jallcom.2019.02.238
53. Braun, R., Rovere, F., Mayrhofer, P.H., Leyensa, C.: Environmental protection of γ-TiAl based alloy Ti-45Al-8Nb by CrAlYN thin films and thermal barrier coatings. Intermetallics. **18**, 4 (2010). https://doi.org/10.1016/j.intermet.2009.09.007
54. Ross, I.M., Rainforth, W.M., Seabourne, C.R., Scott, A.J., Wang, P., Mendis, B.G., Bleloch, A.L., Reinhard, C.: Hovsepian, electron energy loss spectroscopy of Nano-Scale CrAlYN/CrN-CrAlY(O)N/Cr(O)N multilayer coatings deposited by unbalanced Magnetron sputtering. Thin Solid Films. **518**, 18 (2010). https://doi.org/10.1016/j.tsf.2010.03.012
55. Myandoab, M.T., Efeoğlu, İ., Ezirmik, K.V., Totik, Y., Arslan, E., Çiçek, H.: High Temperature Oxidation of CrAlYN CrY Thin Films andAdhesion Properties, ICMCTF (2015). (2015)